



# The oxidized hyaluronic acid hydrogels containing paeoniflorin microspheres regulates the polarization of M1/M2 macrophages to promote wound healing

Jiarui Liu<sup>a,1</sup>, Siqi Chen<sup>b,1</sup>, Zijing Zhang<sup>c</sup>, Xitong Song<sup>c</sup>, Zhiquan Hou<sup>c</sup>, Ziyi Wang<sup>c</sup>, Tao Liu<sup>d</sup>, Liqun Yang<sup>e</sup>, Yunen Liu<sup>a,\*</sup>, Zhonghua Luo<sup>a,\*</sup>

<sup>a</sup> Shuren International College, Shenyang Medical College, No. 146, Huanghe North Street, Shenyang 110034, China

<sup>b</sup> School of Public Health, Shenyang Medical College, No. 146, Huanghe North Street, Shenyang 110034, China

<sup>c</sup> Graduate School, Shenyang Medical College, No. 146, Huanghe North Street, Shenyang 110034, China

<sup>d</sup> University of Michigan, Ann Arbor, School of Pharmacy, Integrated Pharmaceutical Sciences, 428 Church St, Ann Arbor, MI 48109, United States of America

<sup>e</sup> Research Center for Biomedical Materials, Engineering Research Center of Ministry of Education for Minimally Invasive Gastrointestinal Endoscopic Techniques, Shengjing Hospital of China Medical University, Shenyang 110004, China

## ARTICLE INFO

### Keywords:

Wound healing  
Pae-MPs@OHA  
Molecular docking  
NF- $\kappa$ B/NLRP3 signaling pathway  
Macrophage polarization

## ABSTRACT

Controlling excessive inflammation of acute wound is an effective means to shorten the healing time. Therefore, targeted control of the inflammatory response of the wound is a promising therapeutic strategy. In this study, paeoniflorin (Pae) was encapsulated in microspheres and combined with oxidized hyaluronic acid hydrogels to prepare the hydrogel loaded with Pae microspheres (Pae-MPs@OHA) to promote the healing of acute wounds in rats. The results demonstrated that the particle size of the Pae-MPs was  $6.84 \pm 0.51 \mu\text{m}$ , and the positive charge was  $26.87 \pm 1.51 \text{ mV}$ . The uniform spherical structure of the Pae-MPs was observed by TEM. The Pae-MPs@OHA can maintain colloidal state in the range of 0.1–3.16 Hz. FTIR suggested that Pae could be effectively wrapped in MPs, and SEM indicated that the Pae-MPs@OHA had a uniform network pore structure. The Pae-MPs@OHA can realize the sustained release of Pae for 96 h. Biocompatibility experiments showed that the Pae-MPs@OHA hydrogels were safe and available. The Pae-MPs@OHA hydrogels can accelerate wound healing in rats. HE and masson staining suggested that the Pae-MPs@OHA could reduce inflammatory cell infiltration, promote re-epithelialization and collagen formation. The Pae-MPs@OHA could decrease the number of M1 and increase the number of M2 in macrophages, thus regulating the release of inflammatory factor TNF- $\alpha$  and IL-1 $\beta$ . The results of molecular docking and western blot results also confirmed that the Pae-MPs@OHA could reduce the expression of NF- $\kappa$ B, pNF- $\kappa$ B, NLRP3, ASC and pro-caspase-1. These findings suggest that the Pae-MPs@OHA has great potential for application in the treatment of inflammatory wound.

## 1. Introduction

The area of acute wound is large, easy to be interfered, and the wound with poor long-term healing may even become cancerous. Wound healing consists of four stages, including hemostasis, inflammation, proliferation and remodeling [1,2]. Excessive inflammation is the main cause of long-term wound non-healing. Macrophages play multiple roles in wound healing by regulating their own polarization and secretion of inflammatory factors [3,4]. When macrophages are active, they mainly polarize into classical activated M1 (pro-

inflammatory) and alternate activated M2 (anti-inflammatory) [5]. Under normal circumstances, the content of M1 and M2 macrophages is in a state of dynamic balance. In the acute wounds that are difficult to heal, the phenotype conversion of macrophages is not smooth, the function activation is unbalanced, and the mixed polarization state of increasing M1 type and decreasing M2 type appears [6], which leads to the continuous progress of inflammation. The polarization process of macrophages is involved in multiple signaling pathways. Studies have shown that the NF- $\kappa$ B/NLRP3 inflammatory signaling pathway is an important link [7–9]. Therefore, in the field of wound healing, it is a new

\* Corresponding authors.

E-mail addresses: [liuyey990116@163.com](mailto:liuyey990116@163.com) (Y. Liu), [zhonghua\\_2398@163.com](mailto:zhonghua_2398@163.com) (Z. Luo).

<sup>1</sup> These authors contributed equally to this work.

direction to choose appropriate treatment methods to target the NF- $\kappa$ B/NLRP3 signaling pathway to regulate macrophage polarization.

At present, wound treatment is still mainly focused on cleaning the wound, reducing pressure and rebuilding blood circulation, but these treatment methods cannot achieve satisfactory results [10]. Meanwhile, there is a shortage of treatment methods for excessive wound inflammation. Developing effective anti-inflammatory active ingredients from drugs with homologous characteristics of medicine and food to promote skin wound healing without causing side effects is the direction of wound treatment in the future. Peony is a herbaceous plant belonging to the family paeoniaceae and genus paeonia, the scientific name is *Paeonia lactiflora* Pall. In China, peony has been approved as a raw material for the preparation of health foods. Peony is used as an ingredient in tea, porridge and desserts, which can regulate the spleen and stomach, promote blood circulation and collaterals [11]. The active ingredients in peony mainly include paeoniflorin (Pae), oxidized Pae, as well as other alcohols and phenolic substances. It has been reported that Pae has anti-cancer, anti-depression, anti-inflammatory and liver protection effects, and has therapeutic effects on a variety of inflammatory diseases [12]. Pharmacokinetics indicate that Pae is not easily permeable through biofilms and has low bioavailability.

Therefore, it is necessary to construct a delivery system to improve the effect of Pae. Currently, common delivery systems include liposome, microcapsule and hydrogel. Hydrogels have the advantages of wide adaptability, non-toxicity and low price. Hydrogel, as a new dressing in recent years, its special molecular structure can combine with multiple water molecules and has strong liquid absorption ability. In addition, the special structure of the hydrogel can provide a moist healing environment for the wound, which can prevent the wound from being too dry and crusting, preventing skin cells from migrating to the injury site, and is widely used as a wound dressing [13–15]. Meanwhile, hydrogels with specific 3D structures similar to ECMs are essential for cell proliferation as well as nutrient and waste exchange during healing [13–15]. At present, a variety of hydrogels have been used in clinic, such as woulgan hydrogels and fitostimoline hydrogels, but these dressings have not taken targeted treatment for macrophages and inflammatory process.

The hydrogels for regulating inflammation are designed and customized to promote wound healing, which has broad development prospects. Hyaluronic acid (HA) is the most common material in hydrogels, and a large number of hydroxyl and carboxyl groups in the structure can combine with a large number of water molecules through hydrogen bonds, which makes HA obtain excellent water retention. With the advancement of polymerization methods, the HA derivative oxidized hyaluronic acid (OHA) has been further developed as a reparative biomaterial for wound healing [16]. The hydrogels system of HA and its derivatives can be loaded with various therapeutic drugs and living cells for wound healing. Drug carriers play an important role in the construction of drug delivery system. As a sustained-release carrier, microspheres are gradually applied to the field of wound repair, which can control the release rate, improve drug uptake and enhance drug targeting. Dopamine (DA) is derived from bioactive compounds of marine mussels. DA oxidizes to form polydopamine (PDA) under weak base conditions of aerobic moisture, which can be attached to the surface of the material. Mesoporous polydopamine microspheres (PDA-MPs) are easy to prepare [17], and have a large specific surface area to load growth factors, cytokines and proteins [18,19]. Therefore, it is necessary to prepare hydrogel microsphere dressings with uniform particle size, good physical stability and biocompatibility to meet the application of excessive inflammatory wounds.

In this study, Pae loaded microspheres were combined with OHA crosslinked hydrogels to prepare Pae loaded microspheres hydrogels (Pae-MPs@OHA) in this study. The particle size, distribution and zeta potential of the Pae-MPs were measured. The infrared properties, scanning electron microscopy, rheological properties, drug release rate and biocompatibility of the Pae-MPs@OHA were characterized. Acute wound model was established to observe the healing effect of the Pae-

MPs@OHA on the wound in rats (Scheme 1). The mechanism of the Pae-MPs@OHA promoting wound healing was further explored to provide a theoretical basis for the application of the Pae-MPs@OHA on acute wounds.

## 2. Materials and methods

### 2.1. Reagents and chemicals

Paeoniflorin (purity  $\geq 98\%$ ), pluronic F-127 (F127), dopamine hydrochloride, 1,3,5-trimethylbenzene (TMB), oxidized hyaluronic acid (OHA), adipic diazide (ADH) and N-(3-dimethylaminopropyl)-N'-ethylcarbodiimide hydrochloride (EDC) were purchased from Aladdin (Shanghai, China). The calcein AM/PI dual staining kit, PBS, MEM and CCK-8 kits were obtained from Solarbio (Beijing, China). The primary antibodies anti-NF- $\kappa$ B (#8242), pNF- $\kappa$ B (#3033), ASC (#67824) and GAPDH (#97166) were provided by Cell Signaling Technology (MA, USA). The primary anti-NLRP3 (ab263899) and pro-caspase-1 (ab179515) were provided by Abcam (MA, USA). The cDNA Synthesis Kit and SYBR dyes were obtained from Vazyme (Nanjing, China). The primers were obtained from Biotech (Shanghai, China). The IL-1 $\beta$  and TNF- $\alpha$  enzyme-linked immune response (ELISA) test kits were purchased from Enzyme-Linked Biosystems (Shanghai, China).

### 2.2. Preparation of the Pae-MPs@OHA

F127, DA and TMB were dispersed in the mixture of ethanol and water under continuous agitation, the ammonia solution was dropped, and the coarse microspheres were collected by centrifugation. After removing the template, the PDA-MPs were obtained by centrifugation and freeze-drying. 60 mg PDA-MPs was suspended in the water/ethanol mixture, and 30.0 mg of the Pae was added, stirred for 24 h, and the microspheres loaded with the Pae (Pae-MPs) were collected by centrifugation. HA was stirred and dissolved, and ADH was added. After adjusting PH, EDC was added and stirred vigorously, and the solution became gel. 1.44 mg Pae-MPs was added to each mL of hydrogels to prepare the Pae-MPs@OHA.

### 2.3. Material characterization method

#### 2.3.1. Measure the particle size and zeta potential of MPs and the Pae-MPs

Pure water was used to dedilute MPs and the Pae-MPs to 10 mg/mL. The particle size, polymer dispersity index (PDI) and zeta potential of MPs and the Pae-MPs were measured by particle size meter.

#### 2.3.2. Infrared spectrum

The Pae, the MPs and the Pae-MPs were placed in Fourier transform infrared spectroscopy (FTIR), and infrared absorption curves at wavelengths of 400–5000  $\text{cm}^{-1}$  were scanned.

#### 2.3.3. Scanning electron microscope (SEM)

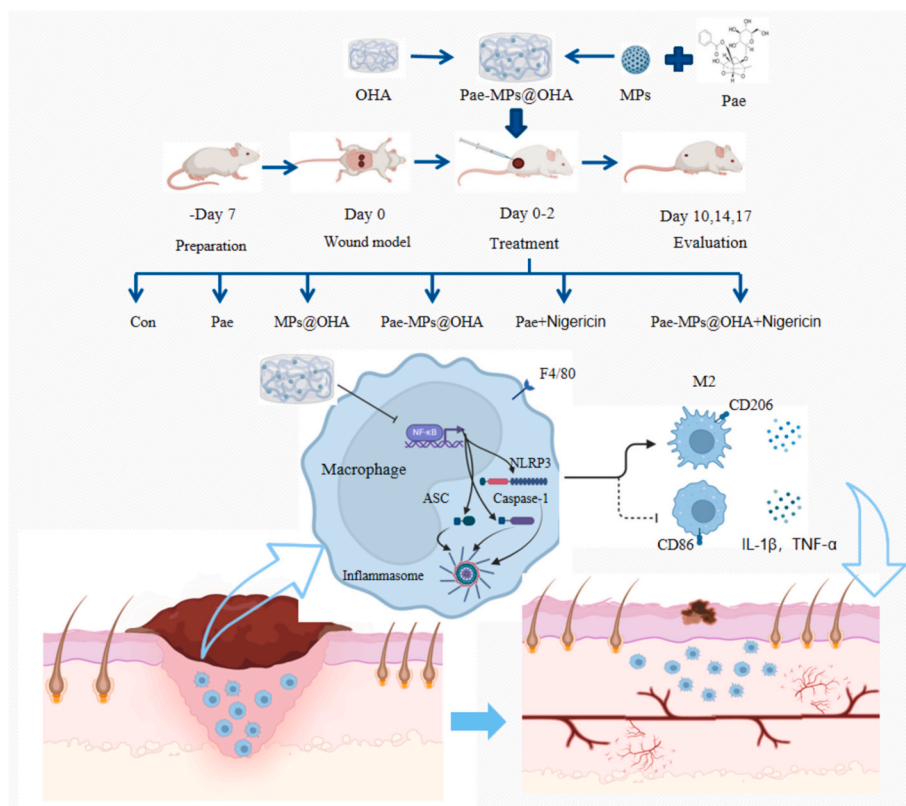
The Pae-MPs, OHA and the Pae-MPs@OHA were freeze-dried, fixed on conductive resin and sprayed with gold, and the surface morphology photos were collected.

#### 2.3.4. Transmission electron microscope (TEM)

The experimental samples were subjected to alcohol ultrasound for 15 min, dropped on the copper net, then tested after air drying.

#### 2.3.5. Detecting the encapsulation efficiency and drug loading rate of the Pae-MPs

Pae was prepared into 0.61 mg/mL solution with ethanol and deionized water, and the OD value was measured by dilution. Then, 4.0 mg mesoporous polydopamine microspheres were added into 3.3 mL Pae solution. After incubation for 24 h, the Pae-MPs were collected by centrifugation and OD value of supernatant was determined. The



**Scheme 1.** Mechanism diagram of the Pae-MPs@OHA promoting acute wound healing in rats.

concentration of the Pae was calculated according to the standard curve of Pae. Then, the encapsulation rate and drug loading rate of microspheres were calculated by the following formula.

$$\text{Encapsulation rate (\%)} = \frac{M - M1}{M} \times 100\%$$

$$\text{Drug loading rate (\%)} = \frac{M - M1}{(M - M1) + M2} \times 100\%$$

M is the amount of Pae input. M1 is the mass of Pae in the remaining supernatant. M2 is the mass added to MPs.

### 2.3.6. *In vitro* release experiment of the Pae-MPs@OHA

2 mL PBS was added to 0.5 mL Pae-MPs@OHA, and PBS was taken out and supplemented every 24 h. The absorbance was measured at the wavelength of 230 nm, and the release amount and cumulative release amount of the Pae were calculated. The cumulative release rate formula was as follows.

$$\text{Cumulative release rate (\%)} = \frac{V \sum_{1}^n C_n}{m} \times 100\%$$

n is the total number of releases collected, V is the volume of the releases collected at each time point (2 mL), C<sub>n</sub> represents the concentration of the releases collected at the n-th time, and m is the mass of the hydrogels loaded the Pae.

### 2.3.7. Detection of rheological properties of hydrogels

The storage modulus (G') and loss modulus (G'') of the MPs@OHA and the Pae-MPs@OHA were tested by dynamic rheometer at 1 % constant strain, 37 °C and frequency range of 0.01–10 Hz.

## 2.4. Determination of biocompatibility of the Pae-MPs@OHA

In this study, the hydrogels extract was co-cultured with L929 cells to

test the biocompatibility of hydrogels. 200 μL MPs@OHA and the Pae-MPs@OHA were sterilized by ultraviolet, then transferred to a 24-well plate, and 1 mL of complete culture medium was added for extraction with 24 h. Pae was diluted to 35 μg/mL. The extract was filtered using a microporous filter membrane.

### 2.4.1. Cell viability assay

Mouse immortalized fibroblasts (L929) were cultured in MEM medium (Solarbio, Beijing, China) containing 10 % fetal bovine serum (Thermo Fisher, MA, USA) at 37 °C and 5 % CO<sub>2</sub>. The cells (5 × 10<sup>3</sup> cells/holes) were cultured in 96-well plates for 24 h and treated with different extracts for 24 h. The cell viability was detected by CCK-8 method at 450 nm. The following formula was used to calculate the survival rate.

$$\text{Cell proliferation rate (\%)} = \frac{OD_{\text{sample}} - OD_{\text{blank}}}{OD_{\text{control}} - OD_{\text{blank}}} \times 100\%$$

OD<sub>sample</sub> represents the absorbance of cells with samples, and OD<sub>control</sub> represents the absorbance of cells without samples, OD<sub>blank</sub> represents the absorbance without cells or samples.

### 2.4.2. Staining of live/dead cells

10 × assay buffer was diluted 10 times with deionized water to obtain 1 × assay buffer. 500 μL of 5 × 10<sup>5</sup>/mL L929 cells were inoculated in the plate, and 500 μL of different groups of extracts were added to each well after adhesion, and the cells were digested and collected 24 h later. The cell precipitation was obtained by digestion and centrifugation, and the cell reached 1 × 10<sup>6</sup>/mL. The cells were incubated with 2 μL Calcein-AM and 5 μL PI, and observed by fluorescence microscope.

### 2.4.3. Scratch assay

L929 cells (5 × 10<sup>4</sup> cells/well) were cultured in a 6-well plate for 24 h, and the plate was scraped with a 200 μL sterile pipette tip to prepare

scratches. The cells were treated with different groups of serum-free extracts and incubated. The microscope with a digital camera was used to observe scratches at 0, 24, 48 and 72 h and take pictures. The image J was used to process the image, repeated 3 times at each time point. The following formula was used to calculate cell relative mobility.

$$\text{Relative migration rate (\%)} = \left(1 - \frac{L_n}{L_0}\right) \times 100\%$$

#### 2.4.4. Test of binding rate of the Pae-MPs@OHA to TNF- $\alpha$ and IFN- $\gamma$

The concentration changes of TNF- $\alpha$  and IFN- $\gamma$  proteins before and after incubation with hydrogel were detected by ELISA kit to explore the ability of hydrogel to capture them. The samples of the MPs@OHA group, Pae group, the Pae-MPs@OHA group were placed in 48-well plates, and 3 parallel samples were set in each group. The solutions of TNF- $\alpha$  protein and IFN- $\gamma$  protein were added and incubated with samples of each group at room temperature. In addition, the pure protein control group was set up. After 24 h, the supernatant was collected and stored in the refrigerator at  $-80^\circ\text{C}$ , then quantitatively detected by the Elisa kit.

#### 2.4.5. In vivo degradation experiment of Pae-MPs@OHA

18 male SD rats, weighing  $200 \pm 10$  g and aged 6–8 weeks, were provided by Beijing Huafukang Biotechnology Co., Ltd. The experimental animals and protocol have been approved by the Animal Protection and Ethics Committee of Shenyang Medical College (Certificate ID SYXY2023091001). The rats were randomly divided into the control group, the MPs@OHA group and the Pae-MPs@OHA group. The SD rats were anesthetized, and their back hair was shaved with an electric shaver. The MPs@OHA and the Pae-MPs@OHA hydrogels were injected subcutaneously into SD rats with syringes. The survival of the rats was observed, the implanted hydrogel and its surrounding tissue were removed 7 and 14 days after injection. The degradation of hydrogel in rats was observed. The surrounding histopathology was analyzed by H&E staining.

### 2.5. Establishing an acute wound model in rats

60 male SD rats [( $200 \pm 10$ ) g, 6–8 weeks old] were purchased from Beijing Huafukang Biotechnology Co., Ltd. The experimental animals and protocol have been approved by the Animal Protection and Ethics Committee of Shenyang Medical College (Certificate ID SYXY2023071201). The rats were randomly divided into the control group, the MPs@OHA group, the Pae group, the Pae-MPs@OHA group, the Pae + nigericin group and the Pae-MPs@OHA + nigericin group, treatment for 3 days. After fasting for 12 h, two acute wounds with a diameter of 1.2 cm were prepared on the back of rats. No treatment was given in the control group. The MPs@OHA group was given 0.5 mL MPs@OHA for each wound. In the Pae group, 51.6  $\mu\text{L}$  paeoniflorin (5 mg/mL) was applied. In the Pae-MPs@OHA group, 0.5 mL Pae-MPs@OHA was applied. The Pae + nigericin group was applied with paeoniflorin, and 4 mg/kg nigericin solution was injected subcutaneously. The Pae-MPs@OHA + nigericin group was injected with nigericin solution while receiving the Pae-MPs@OHA. On the 10th, 14th and 17th day after modeling, serum and wound tissues of rats were taken. The serum IL-1 $\beta$  and TNF- $\alpha$  were detected according to the kit instructions. The wounds of rats were photographed at 0, 4, 8, 12 and 16 days to calculate the healing rate. The following was the formula for calculating the healing rate of rat wounds.

$$\text{Wound closure rate (\%)} = \frac{\text{the area of Day 0} - \text{the area of Day N}}{\text{the area of Day 0}} \times 100\%$$

### 2.6. Histopathological analysis

The wound tissues of 10, 14 and 17 days were dehydrated with xylene and ethanol, and the slices of 3  $\mu\text{m}$  were prepared after paraffin

embedding. HE and masson staining were performed on the sections of each group, and the histopathological changes of the wound were observed by microscope.

### 2.7. Real-time fluorescence quantitative PCR

Total mRNA was extracted by NucleoZOL. The experiment was carried out according to the instruction manual of reverse transcription reagent and fluorescent dye. The relative expression of genes was calculated by  $R = 2^{-\Delta\Delta\text{Ct}}$ . The glyceraldehyde-3-phosphate dehydrogenase was used as the internal reference gene. The primer premier 6.0 was used to design the required primers. Primer sequence was shown in Table S1.

### 2.8. Molecular docking analysis

The structure of Pae was downloaded from PubChem official website (<https://pubchem.ncbi.nlm.nih.gov/>) as a ligand. The protein structures of NF- $\kappa\text{B}$  (7LEQ), NLRP3 (7ALV), ASC (6KIO), and caspase-1 (1BMQ) were obtained from the PDB protein website (<https://www.rcsb.org/>) as the dock-receptor. The receptor protein was imported into SYBYL software for processing to find the active pocket of receptor protein. The ligand was introduced into SYBYL software and docked with the active pocket of receptor protein. The total score and cscore parameters were used to evaluate the interconnection capability. Discovery Studio software was used to visualize and analyze the interaction between ligand and receptor protein.

### 2.9. Western blot

The total protein of wound tissues was extracted with RIPA lysate. The total protein was quantified by BCA kit. The proteins were isolated by SDS-PAGE gel electrophoresis and transferred to PVDF membranes. The membrane was sealed with skimmed milk powder, then incubated with the primary antibodies of NF- $\kappa\text{B}$ , pNF- $\kappa\text{B}$ , NLRP3, pro-caspase-1, ASC and GAPDH. After washing, it was incubated with the corresponding secondary antibody. ECL developer was used to emit light on the luminescent plate.

### 2.10. Statistical analysis

Graphpad Prism 8.0 was used to analyze the results, which were expressed as mean  $\pm$  standard deviation (SD). One-way ANOVA and two-way ANOVA was used to analyze the data of each group.  $p < 0.05$  was considered statistically significant.

## 3. Results

### 3.1. Preparation and characterization of the Pae-MPs@OHA dressing

The preparation process and morphology of the Pae-MPs@OHA were shown in Fig. 1A and B, indicating that the Pae-MPs@OHA was successfully prepared. In Fig. 1C, the Pae-MPs@OHA had good viscosity and elasticity and can adhere to the skin and spleen of rats. As shown in Table 1, the particle size of the Pae-MPs was  $6.84 \pm 0.51$   $\mu\text{m}$ , the PDI was  $0.16 \pm 0.07$ , and the zeta potential was  $26.87 \pm 1.51$  mV. It was suggested that it had uniform particle size and good stability. The rheological experiment displayed that the Pae-MPs@OHA can maintain the colloidal morphology of hydrogels in the range of 0.1–3.16 Hz, and had good rheological properties (Fig. 1D).

### 3.2. Load and release of Pae in the Pae-MPs@OHA

As shown in Fig. 2A, the Pae infrared spectrum indicated that the absorption peak of C=O stretching vibration was at  $1701\text{ cm}^{-1}$ .  $1266\text{ cm}^{-1}$  was the absorption peak of C—O stretching vibration in ester

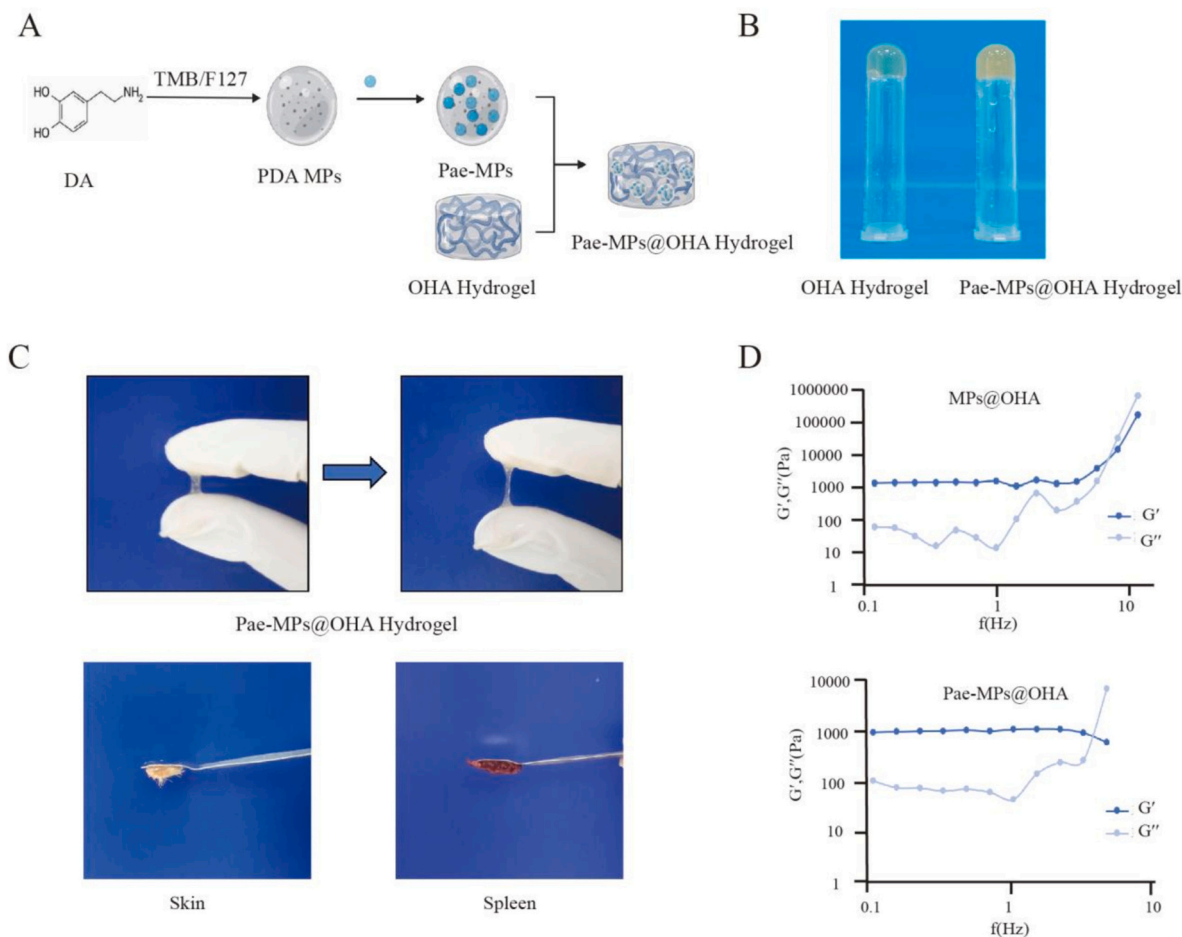


**Fig. 1.** Preparation and characterization of the Pae-MPs@OHA. (A) Preparation process of the Pae-MPs@OHA hydrogels. (B) The physical drawings of OHA crosslinked hydrogels and the Pae-MPs@OHA hydrogels. (C) Evaluation of adhesion properties of the Pae-MPs@OHA hydrogels. (D) Rheological properties of OHA hydrogels and the Pae-MPs@OHA hydrogels.

**Table 1**  
Particle size and distribution of MPs and Pae-MPs.

Sample	Size (nm)	PDI	Zeta potential (mV)
MPs	1715.67 ± 195.16	0.31 ± 0.13	-25.72 ± 1.24
Pae-MPs	6842.83 ± 505.81	0.16 ± 0.07	26.87 ± 1.51

group (–COOR). The stretching vibration absorption peaks of C–O were  $1174\text{ cm}^{-1}$  and  $1077\text{ cm}^{-1}$ . The stretching vibration absorption peak of C–O–C was at  $1046\text{ cm}^{-1}$ . The absorption peak at  $719\text{ cm}^{-1}$  was related to the flexural vibration of single-substituted benzene C–H. The bending vibration absorption peak of C–O–C in epoxy compounds was at  $570\text{ cm}^{-1}$ .

From the infrared spectrum of MPs, it can be observed that the stretching vibration at  $2876\text{ cm}^{-1}$  corresponds to C–H. At  $1405\text{ cm}^{-1}$  and  $1317\text{ cm}^{-1}$ , there were S=O stretching vibration absorption peaks in sulfonic acid group (–SO<sub>3</sub>H). The absorption peak of S–O stretching vibration in sulfonic acid group (–SO<sub>3</sub>H) was at  $1023\text{ cm}^{-1}$ . The absorption peaks of S–O bending vibration in –SO<sub>3</sub>H were at  $560\text{ cm}^{-1}$  and  $461\text{ cm}^{-1}$ . By comparing the FTIR spectra of the Pae-MPs, we can see that  $715\text{ cm}^{-1}$  was the bending vibration absorption peak of single substituted benzene C–H in the Pae-MPs spectra.  $570\text{ cm}^{-1}$  was the characteristic absorption peak of C–O–C bending vibration of Pae. The absorption peaks of S=O and S–O are at  $1405\text{ cm}^{-1}$  and  $1026\text{ cm}^{-1}$ .  $447\text{ cm}^{-1}$  was the characteristic absorption peak of S–O bending vibration of MPs, which indicated that the Pae-MPs can contain the Pae and MPs components. The above infrared spectrum results confirmed

that the Pae could be effectively wrapped in MPs.

The particle microstructure of MPs and the Pae-MPs observed by TEM was shown in Fig. 2B. MPs and the Pae-MPs had uniform spherical structure, and the particle size of the Pae-MPs was increased due to the load of the Pae. As shown in Fig. 2C, the OHA crosslinked hydrogels had a three-dimensional network structure, which can achieve good permeability of the wound surface and provide space for loading the Pae-MPs. Furthermore, the Pae-MPs@OHA also had a uniform reticular pore structure, and the load of the Pae-MPs was observed in the enlarged view. In this study, we determined that the concentration of the Pae input was  $458.5\text{ }\mu\text{g/mL}$ , and the concentration of the Pae in the remaining supernatant was  $202.7\text{ }\mu\text{g/mL}$ . After calculation, the encapsulation rate of the Pae in the Pae-MPs was 55.8%, and the drug loading rate was 17.4%. In vitro drug release (Fig. 2D–E), the Pae-MPs@OHA can release the Pae and reach the maximum release rate within 24 h. The cumulative release rate within 24 h was 64.8%, which can be released for 96 h. The cumulative release of 0.5 mL Pae-MPs@OHA was  $74.85\text{ }\mu\text{g}$ . Then, it was calculated that the concentration of the Pae in the Pae-MPs@OHA was  $311.6\text{ }\mu\text{M}$ . Studies have shown that the concentration of Pae in [20] hydrogels is 250–500  $\mu\text{M}$ , which has a good therapeutic effect on the wound surface, so this concentration is selected for follow-up study.

### 3.3. Biocompatibility of the Pae-MPs@OHA hydrogels

The cytocompatibility of materials is critical for wound dressings. Skin fibroblasts, as the main cells of wound healing, participate in the

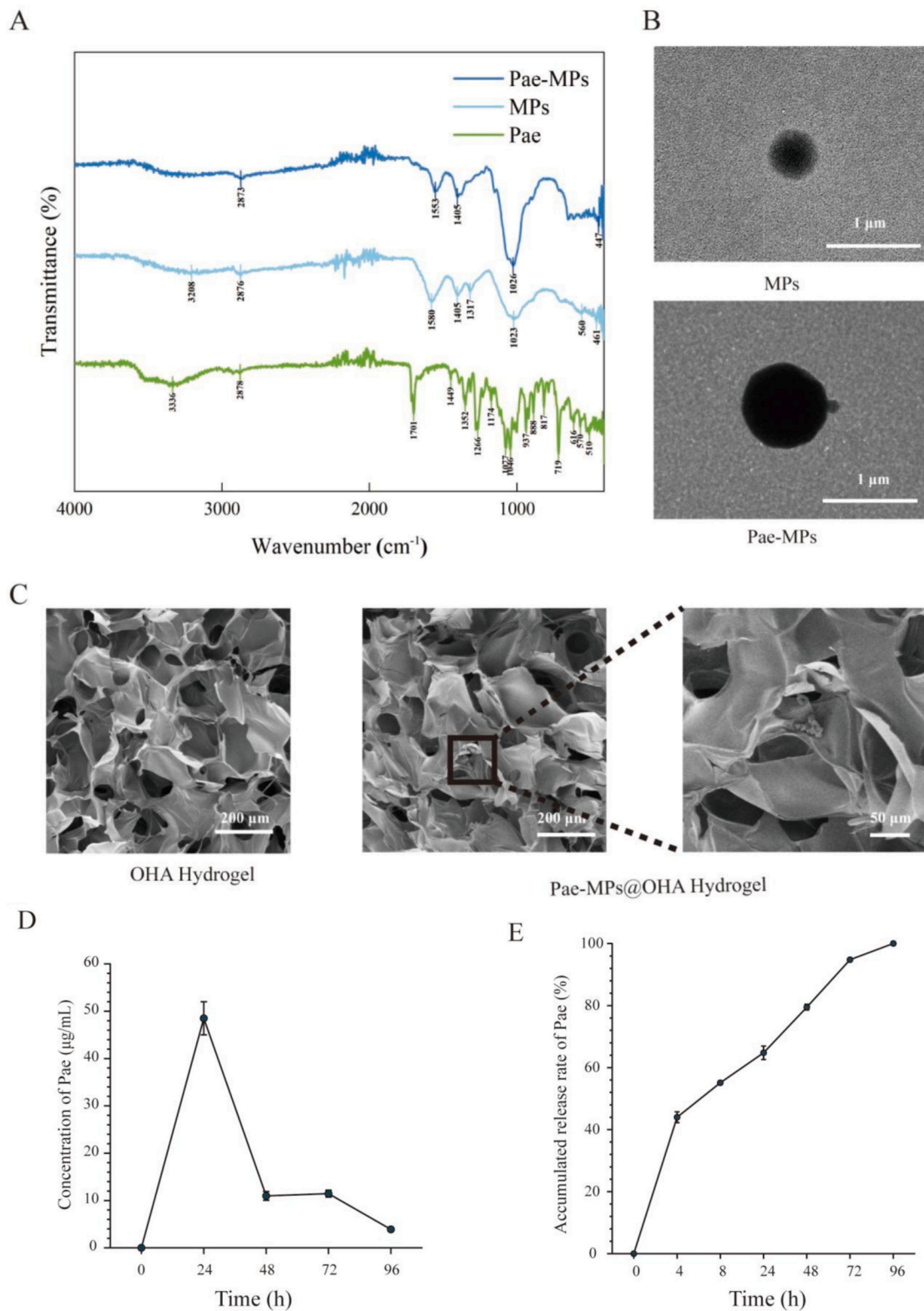


**Fig. 2.** Drug loading and release in the Pae-MPs@OHA hydrogels. (A) FTIR characterization of the Pae-MPs, the Pae and the MPs. (B) TEM structures of the MPs and the Pae-MPs. (C) SEM structures of the the OHA hydrogels, the Pae-MPs@OHA hydrogels. (D) The Pae-MPs@OHA for daily sustained drug release. (E) Cumulative drug release rate of the Pae-MPs@OHA.

whole process of wound healing. In this study, we prepared the Pae-MPs@OHA extract and co-cultured it with L929 cells to observe the cytotoxicity. Fig. 3A–B indicated that the fluorescence staining effect of L929 cells co-cultured with the Pae, the MPs@OHA and the Pae-MPs@OHA extracts for 24 h. Compared with the control group, there

was no significant difference in live cells (green) among the extraction solution groups, with only a few normal dead cells (red) present. As shown in Fig. 3C, compared to the control group, the cell viability of each extraction solution group showed an increasing trend. Meanwhile, the Pae-MPs@OHA had a significant effect on the proliferation of L929

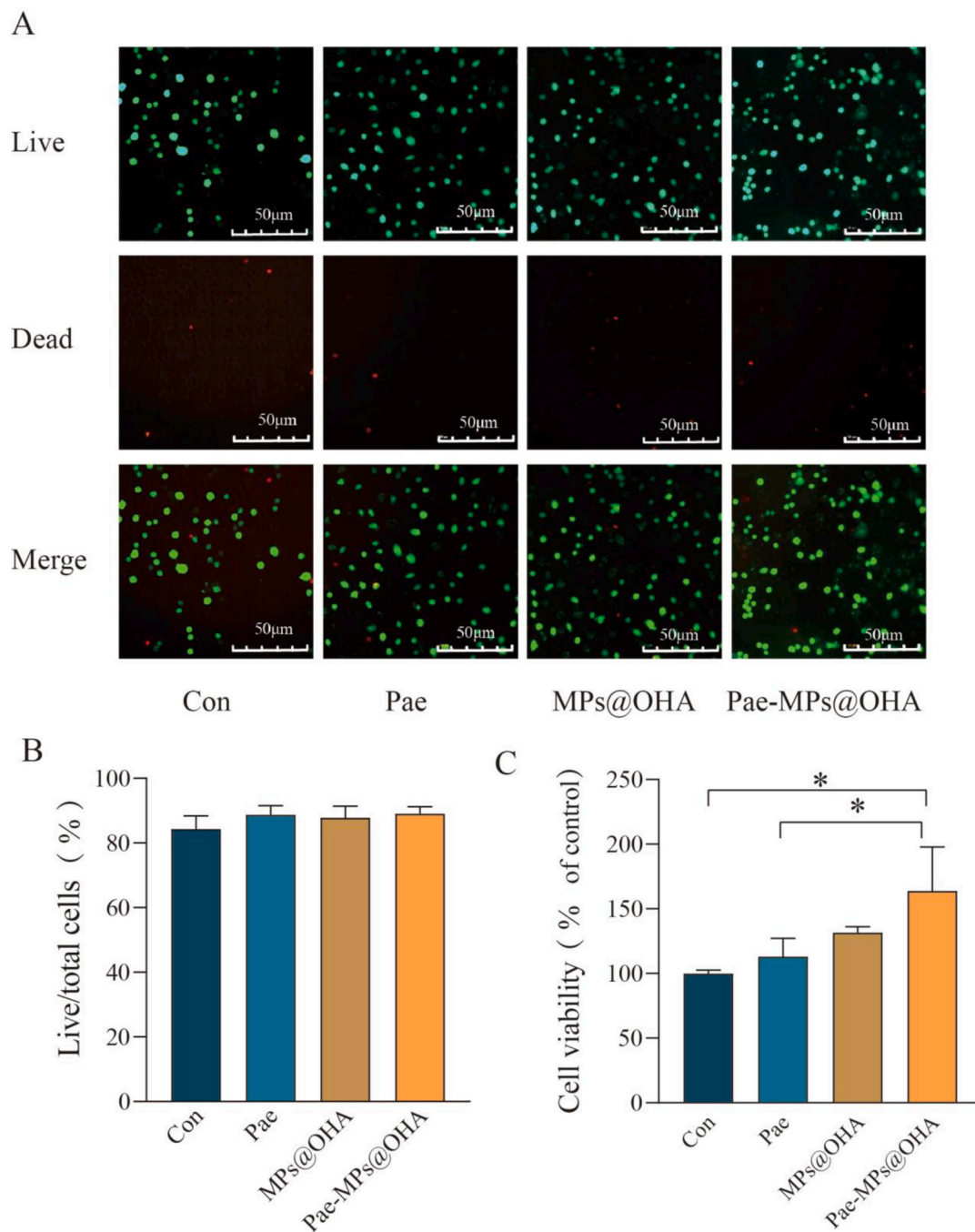


**Fig. 3.** Biocompatibility of the Pae-MPs@OHA. (A) Live/dead cell staining diagrams of cells. (B) Live/dead cell staining statistics. (C) Cell viability was measured by CCK-8 assay. The data were presented as mean  $\pm$  SD ( $n = 3$ ). \* $p < 0.05$ .

cells ( $p < 0.05$ ). These results suggested that the Pae-MPs@OHA had good cell biocompatibility. Therefore, the Pae-MPs@OHA had excellent biocompatibility and had the potential to become a reliable wound dressing.

Cell migration is a key step in wound healing. Therefore, we evaluate the migration ability of hydrogel through cell scratch test. As implied in Fig. 4A–C, the experimental results showed that the Pae did not show a significant effect on fibroblast migration. Compared with the control group, the MPs@OHA and the Pae-MPs@OHA were significantly promoted cell migration at 48 h and 72 h ( $p < 0.01$ ), while only the Pae-MPs@OHA displayed a significant promotion at 24 h ( $p < 0.01$ ). This indicated that the Pae-MPs@OHA can effectively enhance fibroblast migration, thereby accelerating the wound healing process. The TNF- $\alpha$

and IFN- $\gamma$  are inflammatory factors that activate the polarization of M1-type giant cells. The effect of the Pae-MPs@OHA on the polarization of macrophages was evaluated by measuring the clearance effect of these two factors. As displayed in Fig. 4D, compared with the MPs@OHA group, the Pae-MPs@OHA group had a higher binding rate of TNF- $\alpha$ , with a clearance rate of about 68%. From Fig. 4E, it can be seen that compared to the Pae and the MPs@OHA groups, it was found that the Pae-MPs@OHA hydrogels could significantly remove IFN- $\gamma$  ( $p < 0.05$ ).

In vivo safety and degradability of hydrogels are important properties to avoid surgical risks and pain. After injection, the survival of rats was observed, and it was found that the survival of rats was good and was not affected, and no death occurred in each group. According to the H&E staining results in Fig. 4F, there was still a gap between the

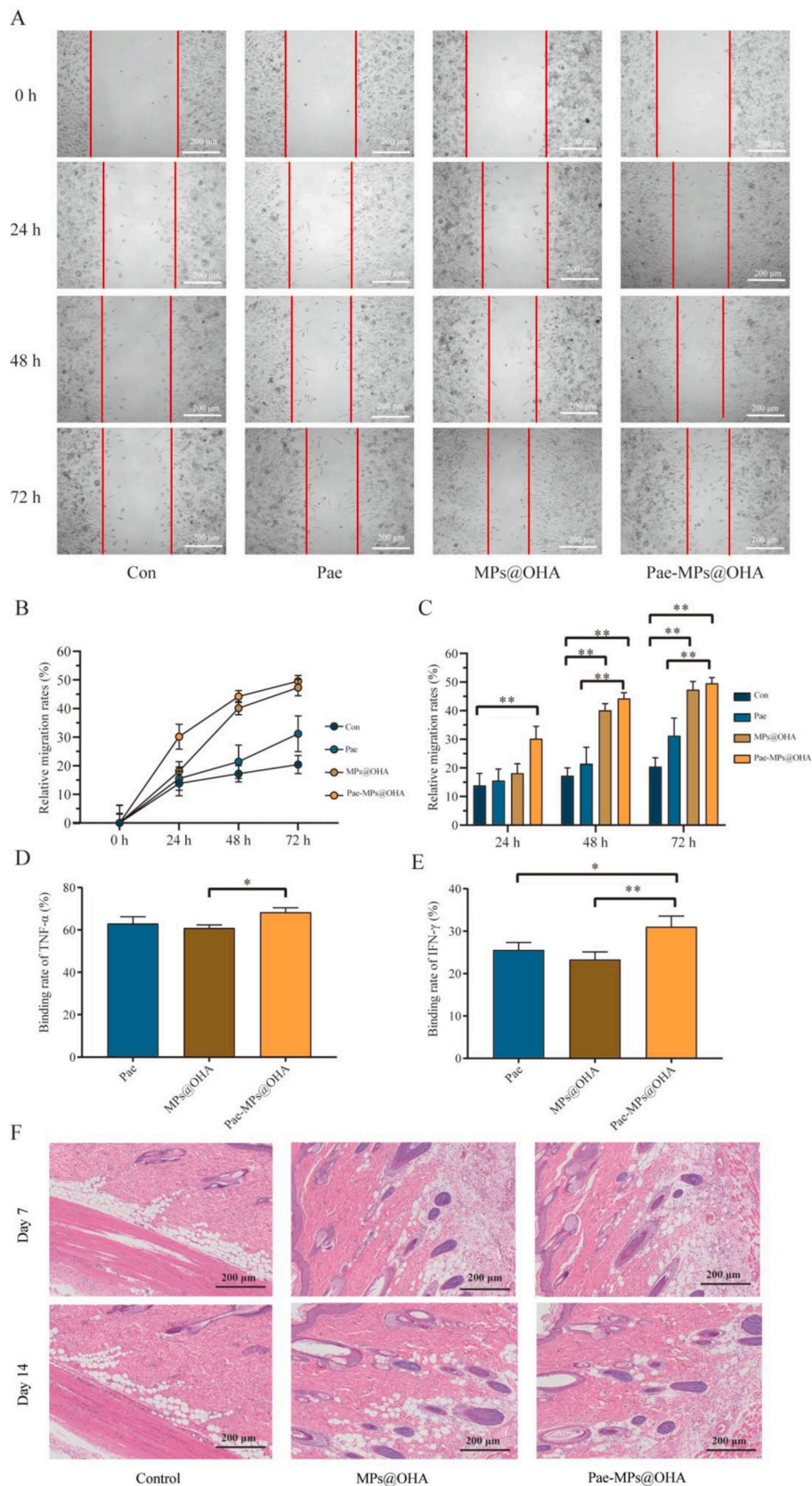


**Fig. 4.** The Pae-MPs@OHA hydrogels promote cell migration in vitro. (A) Representative micrographs of wound edges in scratch measurements at 0, 24, 48, and 72 h in each group. (B–C) Quantitative plots of cell migration rates for each group at the same time point. (D–E) In vitro binding rate of the Pae-MPs@OHA hydrogels to TNF- $\alpha$  and IFN- $\gamma$ . (F) HE staining results of in vivo degradation experiment of the Pae-MPs@OHA hydrogels. The data were presented as mean  $\pm$  SD (n = 3). \* $p$  < 0.05, \*\* $p$  < 0.01.

hydrogel and the surrounding tissues 7 days after injection, and slight inflammatory infiltration appeared in the surrounding tissues. At 14 days, the inflammatory infiltration was significantly weakened, and the surrounding tissues of the hydrogel was close to that of the control group.

### 3.4. Effect of the Pae-MPs@OHA hydrogels on wound healing in rats

As shown in Fig. 5, the Pae, the MPs@OHA and the Pae-MPs@OHA all promoted wound healing compared to the control group, among which the Pae-MPs@OHA had the fastest healing speed (days 4 and 8,  $p < 0.05$ ). Nigericin is an activator of NLRP3, which can trigger inflammatory reaction. The result was indicated in Fig. 5A that the wound healing speed of both groups was delayed after nigericin injection. After injection of nigericin, the rate of wound healing after the Pae-

MPs@OHA treatment was accelerated compared with the Pae group (on the 4th day,  $p < 0.01$ ). As can be seen from Fig. 5B–C, we found that the effect of the Pae-MPs@OHA on wound healing was more significant than that of other groups.

### 3.5. Effect of the Pae-MPs@OHA hydrogels on wound histopathology in rats

The results of HE staining were shown in Fig. 6A. On the 10th and 14th day, the epidermal layer in the control group was incomplete with a large number of inflammatory cells. After treatment with the Pae, the MPs@OHA and the Pae-MPs@OHA, the process of reepithelialization was accelerated, the number of inflammatory cells was reduced. The HE staining results on the 17th day indicated that compared to the control group, the epidermis of the Pae, the MPs@OHA and the Pae-MPs@OHA

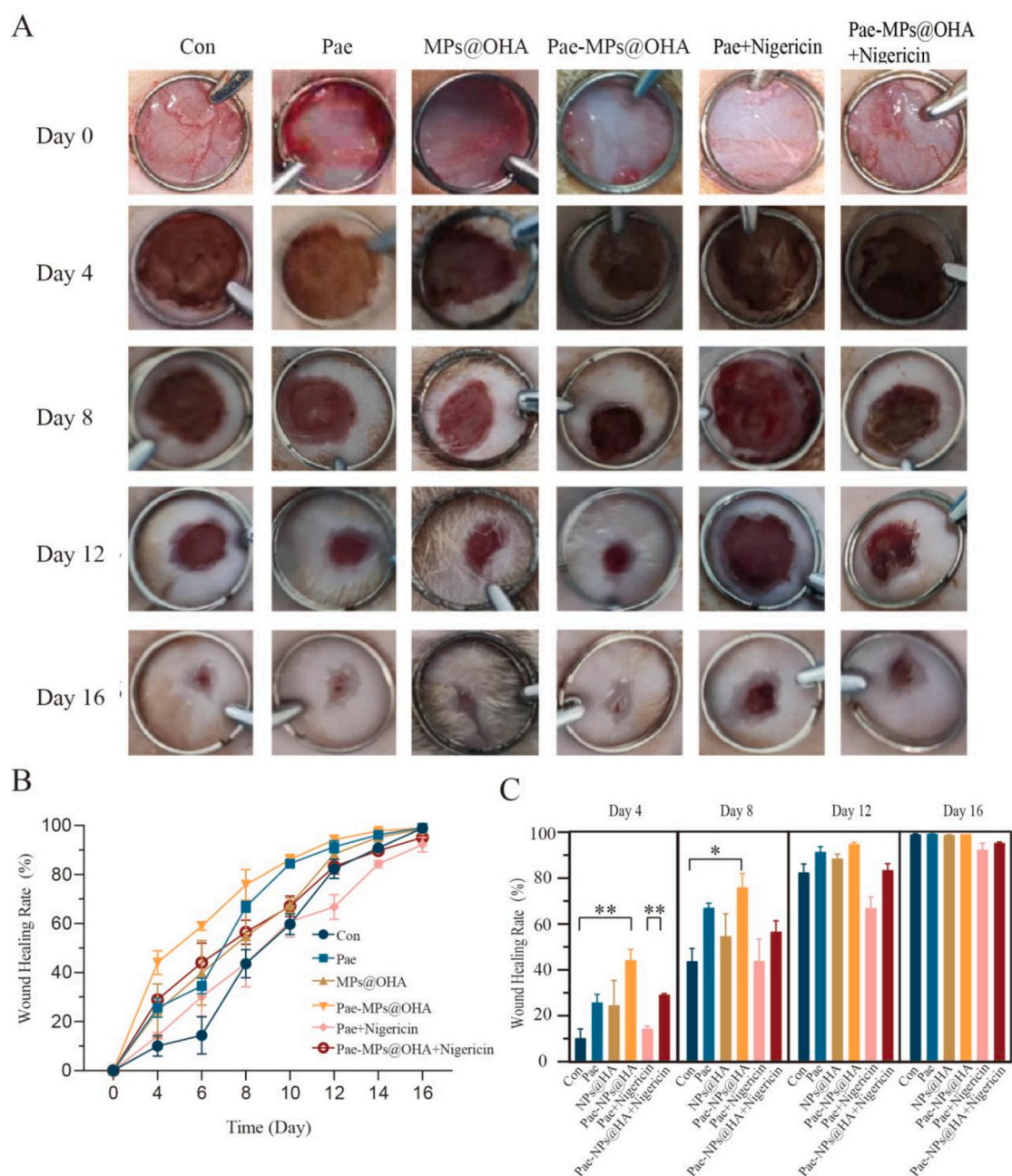


**Fig. 5.** The Pae-MPs@OHA hydrogels promotes healing of acute wounds. (A) Morphological observation of wound healing in each group at different time points after trauma. (B–C) Wound healing rate and statistical analysis of each group at different time points after trauma. \* $p < 0.05$ , \*\* $p < 0.01$ .

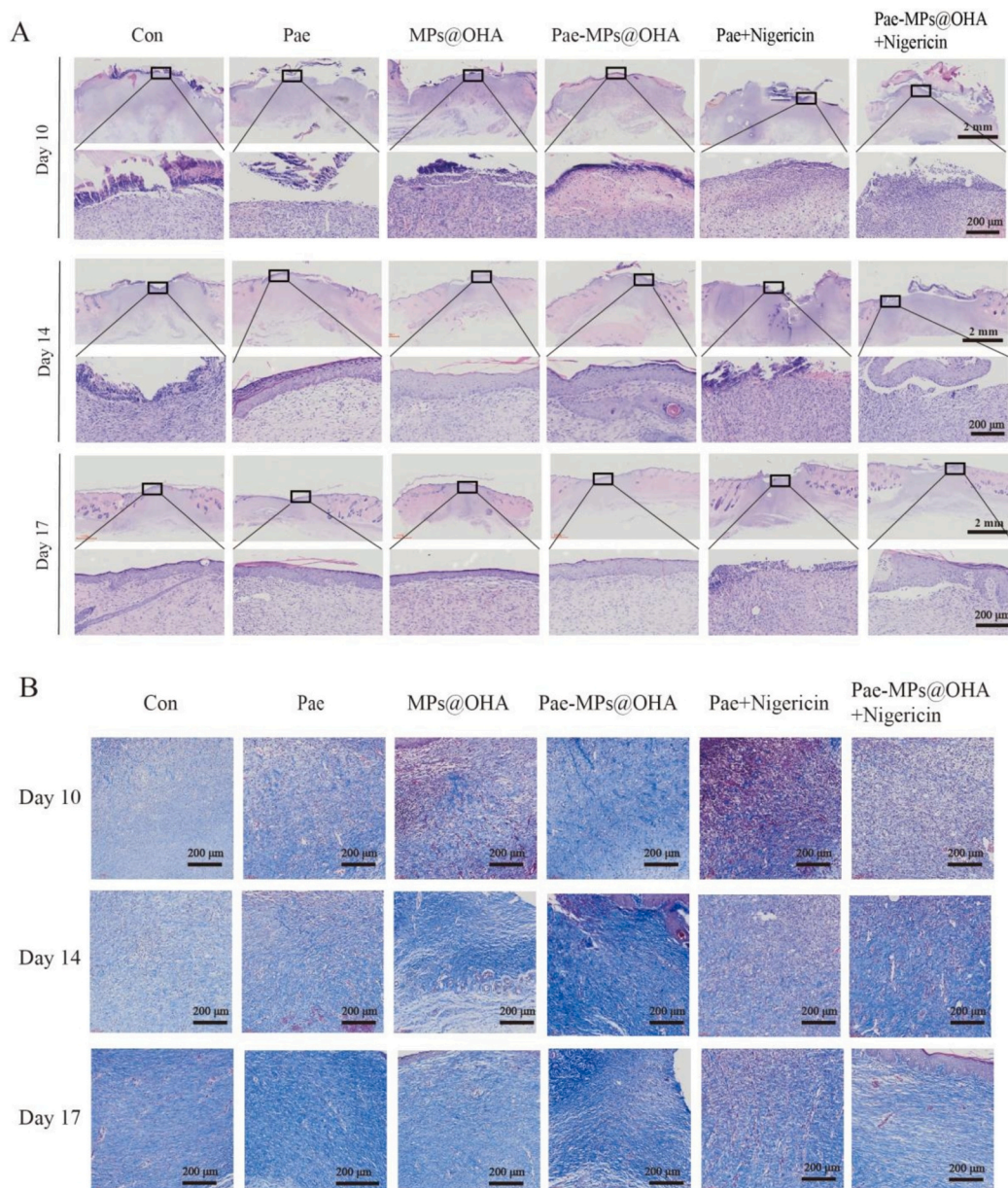


**Fig. 6.** The Pae-MPs@OHA hydrogels promotes wound regeneration and collagen synthesis in the rats. (A) H&E staining was performed in each group at different time points after trauma. Masson staining was performed in each group at different time points after traum.

were complete, and the re-epithelization degree of the Pae-MPs@OHA group was the highest. After injection of nigericin, HE staining showed that on the 10th day, the Pae-MPs@OHA + nigericin and the Pae + nigericin groups had serious inflammatory infiltration and significantly increased inflammatory cells, and no re-epithelization was established. On days 14 and 17, the epidermis of the Pae-MPs@OHA + nigericin group was gradually improved and the inflammatory cells on the wound were reduced, but the epidermis of the Pae + nigericin group has not been completely established.

Masson staining results (Fig. 6B) demonstrated that on the 10th and 14th days of wound healing, collagen fibers in the control group were less stained and arranged sparsely and disordered. After treatment with the Pae, the MPs@OHA and the Pae-MPs@OHA, the collagen fibers were dyed neatly and with uniform density, and the Pae-MPs@OHA group had the best effect. On the 17th day of wound healing, the arrangement of collagen fibers in each group tended to be orderly, and the difference between the groups was decreased. After injection of nigericin, the arrangement of collagen fibers in the Pae-MPs@OHA + nigericin group

gradually tended to be orderly with the prolongation of healing time (on the 10th, 14th and 17th day) compared to the Pae + nigericin group.

### 3.6. Effects of the Pae-MPs@OHA hydrogels on IL-1 $\beta$ and TNF- $\alpha$

Inflammatory factors, as small proteins with extensive biological activities, play an important role in the progression of inflammation. As shown in Fig. 7A–B, the contents of TNF- $\alpha$  and IL-1 $\beta$  in the serum of each group were detected at the 14th and 17th day. The expression of IL-1 $\beta$  in the Pae group, the MPs@OHA group and the Pae-MPs@OHA group was decreased compared to the control group. On the 17th day, the decrease of IL-1 $\beta$  in the Pae group ( $p < 0.05$ ) and the Pae-MPs@OHA group was significantly different from that in the control group ( $p < 0.01$ ). Compared with the control group, the expression of TNF- $\alpha$  in the Pae, the MPs@OHA and the Pae-MPs@OHA groups was declined. The Pae group and the Pae-MPs@OHA group were significantly decreased ( $p < 0.05$ ) in comparison to the control group. Compared to the control group, the expressions of TNF- $\alpha$  and IL-1 $\beta$  in the Pae + nigericin group

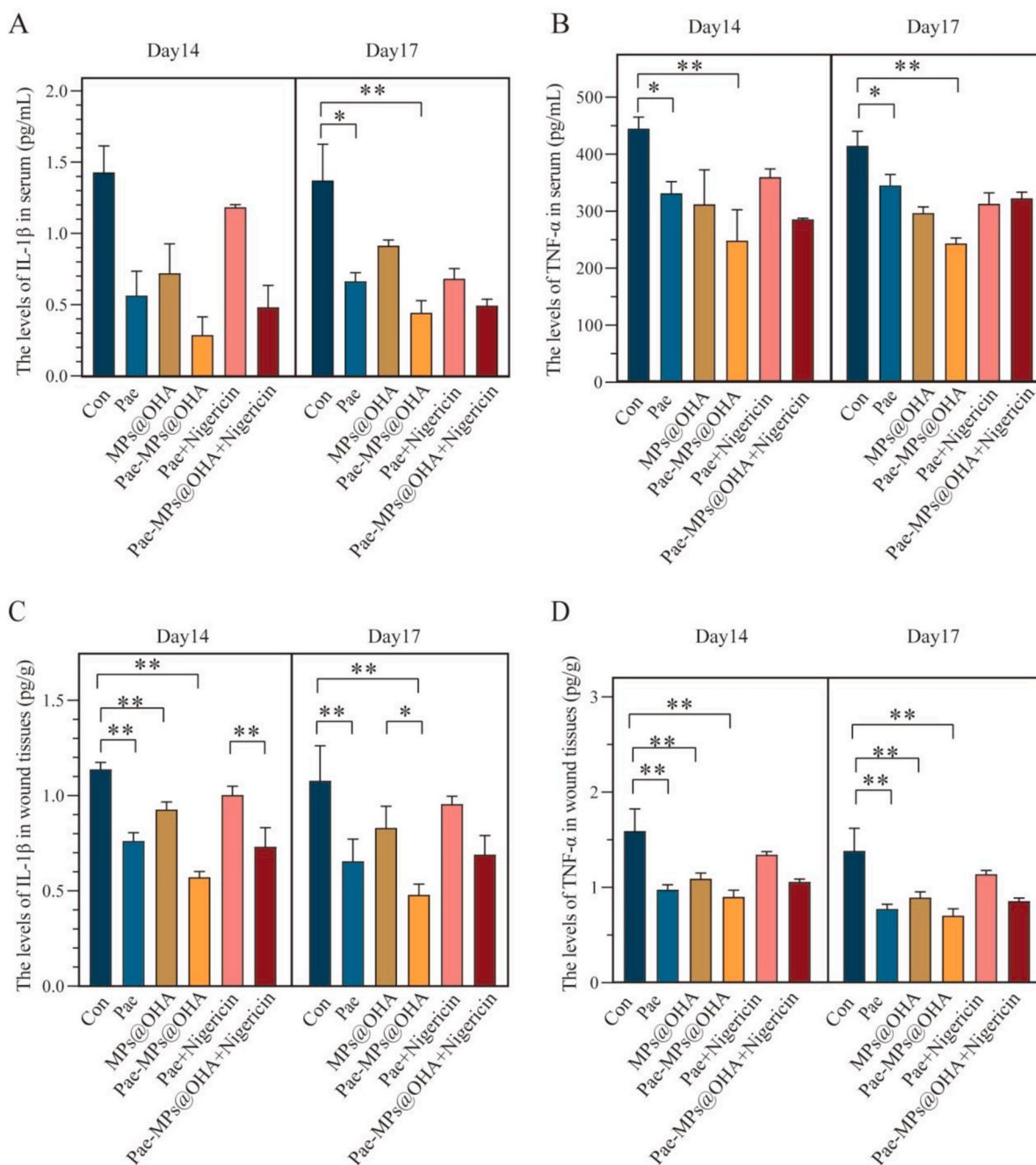


**Fig. 7.** The Pae-MPs@OHA hydrogels can reduce the content of TNF- $\alpha$  and IL-1 $\beta$  in serum of rats. (A–B) The changes and statistical analysis of TNF- $\alpha$  and IL-1 $\beta$  levels in the serum at different time points after trauma in each group. (C–D) The changes and statistical analysis of TNF- $\alpha$  and IL-1 $\beta$  levels in the wound tissues at different time points after trauma in each group. \* $p < 0.05$ , \*\* $p < 0.01$ .

and the Pae-MPs@OHA + nigericin group was also decreased on days 14 and 17. The results in Fig. 7C showed that compared with the control group, the expression level of inflammatory factor IL-1 $\beta$  in wound tissues of rats in the Pae-MPs@OHA group was significantly decreased on the 14th and 17th days ( $p < 0.01$ ). Moreover, compared with the MPs@OHA group, the inflammatory factor IL-1 $\beta$  of wound tissues in the Pae-MPs@OHA group was more sensibly reduced at the 17th day ( $p < 0.01$ ). As shown in Fig. 7D, compared to the control group, the expression of TNF- $\alpha$  in the Pae group, the MPs@OHA group and the Pae-MPs@OHA group was obviously decreased on the 14th and 17th days, with a greater decrease in the Pae-MPs@OHA group.

### 3.7. Effect of the Pae-MPs@OHA hydrogels on phenotypic polarization of macrophages

The balance of M1/M2 macrophages is crucial in wound healing process. In order to explore the regulatory effect of the Pae-MPs@OHA on macrophages in wound tissues, M1 macrophage surface marker CD86 and M2 macrophage surface marker CD206 were selected for subsequent studies. Fig. 8 displayed that compared with the control group, the expression of CD86 in the Pae, the MPs@OHA and the Pae-MPs@OHA groups was decreased and the expression of CD206 was increased. On days 10, compared with the control group, the expression of CD206 in the Pae-MPs@OHA group was dramatically increased ( $p < 0.05$ ). Subcutaneous injection of nigericin into wound tissues will stimulate the

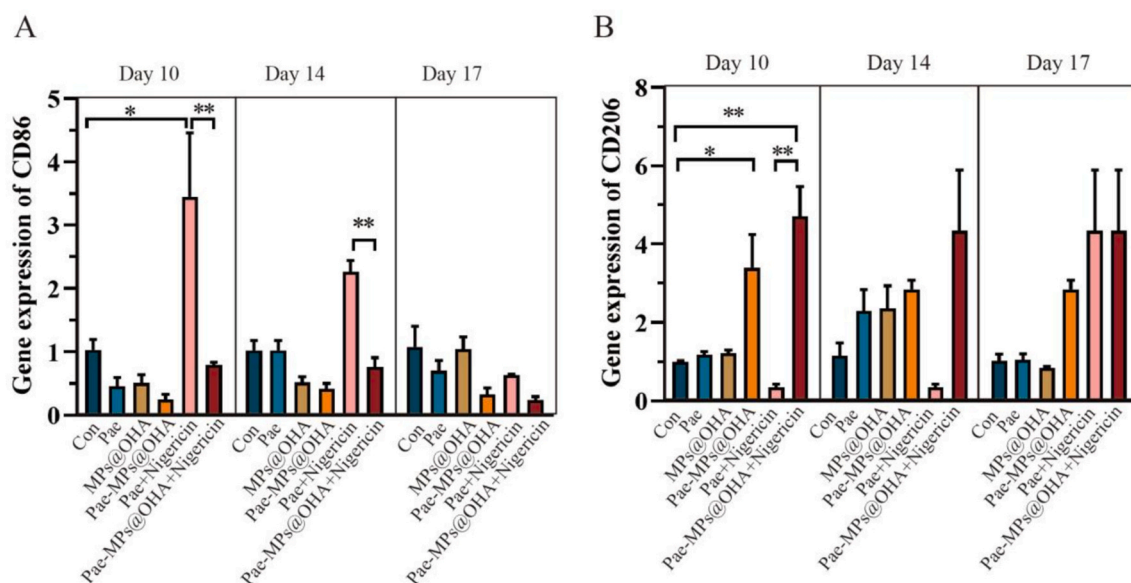


**Fig. 8.** The Pae-MPs@OHA hydrogels regulates the number of M1/M2 macrophages in the rat wounds. (A–B) The expression of CD86 and CD206 mRNA in the wound tissues of 10, 14 and 17 day. GAPDH was used as the internal parameter. \* $p < 0.05$ , \*\* $p < 0.01$ .

immune process. The Pae-MPs@OHA + nigericin group reversed the increase of CD86 mRNA compared to the Pae + nigericin group on the 10th and 14th days, which was significant ( $p < 0.01$ ). The mRNA expression of CD206 in the Pae + nigericin group was low, while the gene expression in the Pae-MPs@OHA + nigericin group was increased, and the expression was significant on the 10th day ( $p < 0.01$ ). Moreover, compared with the control group, the Pae-MPs@OHA + nigericin group had a significant increase in CD206 mRNA ( $p < 0.01$ ). With the extension of wound healing time, the differences of CD86 and CD206 expression levels among all groups was gradually decreased.

### 3.8. Molecular docking results of the Pae

The polarization imbalance between macrophage M1 proinflammatory phenotype and M2 anti-inflammatory phenotype is one of the important mechanisms that cause persistent wound inflammation. Targeted regulation of macrophages can effectively improve the inflammatory status of wounds and promote wound healing. Studies have shown that the NF- $\kappa$ B/NLRP3 signaling pathway is an important signaling pathway regulating M1/M2 phenotype transformation in macrophages [7–9]. Thus, the binding activity of the Pae with NF- $\kappa$ B, NLRP3, ASC and caspase-1 was analyzed by molecular docking. When total score  $> 4$  and cscore  $> 3$ , the ligand has good binding activity with the receptor. The results in the Table 2 demonstrated that the Pae had good binding ability with NF- $\kappa$ B, NLRP3, ASC and caspase-1. The results in Fig. 9 displayed that Pae formed hydrogen bonds, C–H bonds, alkyl groups, with target proteins, and the binding had high stability.

### 3.9. Effect of the Pae-MPs@OHA hydrogels on NF- $\kappa$ B/NLRP3 signaling pathway

Based on the results of molecular docking, this part will continue to

**Table 2**  
Molecular docking score table of Pae with NF- $\kappa$  B, NLRP3, caspase-1 and ASC.

Receptor	Total_Score	CSCORE
NF- $\kappa$ B (7LEQ)	5.51	4
NLRP3 (7ALV)	7.64	4
ASC (6KIO)	7.55	5
Caspase-1 (1BMQ)	4.47	4

explore the regulatory effect of the Pae-MPs@OHA on the NF- $\kappa$ B/NLRP3 signaling pathway in the rat wound tissues. In the Fig. 10, at days 10, 14 and 17, the expressions of NF- $\kappa$ B, pNF- $\kappa$ B, NLRP3, ASC and pro-caspase-1 in the Pae, the MPs@OHA and the Pae-MPs@OHA groups were decreased compared with those in the control group. On the 10th day (Fig. 10A), the expressions of pNF- $\kappa$ B, NLRP3, pro-caspase-1 and ASC in the Pae-MPs@OHA group were sensibly decreased ( $p < 0.05$ ) compared with the control group. Fig. 10B indicated that on day 14, compared with the control group, the expressions of NF- $\kappa$ B, pNF- $\kappa$ B and NLRP3 in the Pae-MPs@OHA group were significantly decreased ( $p < 0.05$ ). Moreover, compared with the Pae group, the decrease of pNF- $\kappa$ B in the Pae-MPs@OHA group was more significant ( $p < 0.05$ ). As shown in Fig. 10C, the expressions of pNF- $\kappa$ B, NLRP3 and pro-caspase-1 in the Pae-MPs@OHA group were prominently declined on day 17 in compare with those for the control group ( $p < 0.05$ ). Compared to the Pae + nigericin group, the expressions of NLRP3 and ASC in the Pae-MPs@OHA + nigericin group were significantly decreased ( $p < 0.05$ ). The results of western blot suggested that NF- $\kappa$ B/NLRP3 signaling pathway was activated in the control group, and the Pae-MPs@OHA group had the most significant inhibitory effect.

## 4. Discussion

Acute wounds are caused by a variety of external factors, the injury area is large, the course of disease is long, and it is easy to cause a series of adverse reactions. The transition from the inflammatory stage to the proliferative stage is a key turning point that determines wound healing [21–23]. Therefore, it is very important to explore the mechanism of wound inflammation and find effective therapeutic means to improve the inflammatory response of wound to shorten the healing time.

With the application of hydrogels more and more widely, simply improving the mechanical properties of hydrogels cannot meet the practical requirements. Functional hydrogels can realize the diversification of functions by loading drugs. In this study, the Pae was wrapped in mesoporous PDA-MPs and loaded on OHA crosslinked hydrogels to prepare the Pae-MPs@OHA. The Pae-MPs@OHA combined the advantages of the Pae with hydrogels to make hydrogels with anti-inflammatory active ingredients. In our study, hyaluronic acid monomers were chemically bonded to form oxidized hyaluronic acid cross-linked hydrogels through the action of chemical crosslinking agents ADH and EDC. The oxidized hyaluronic acid crosslinked hydrogel has

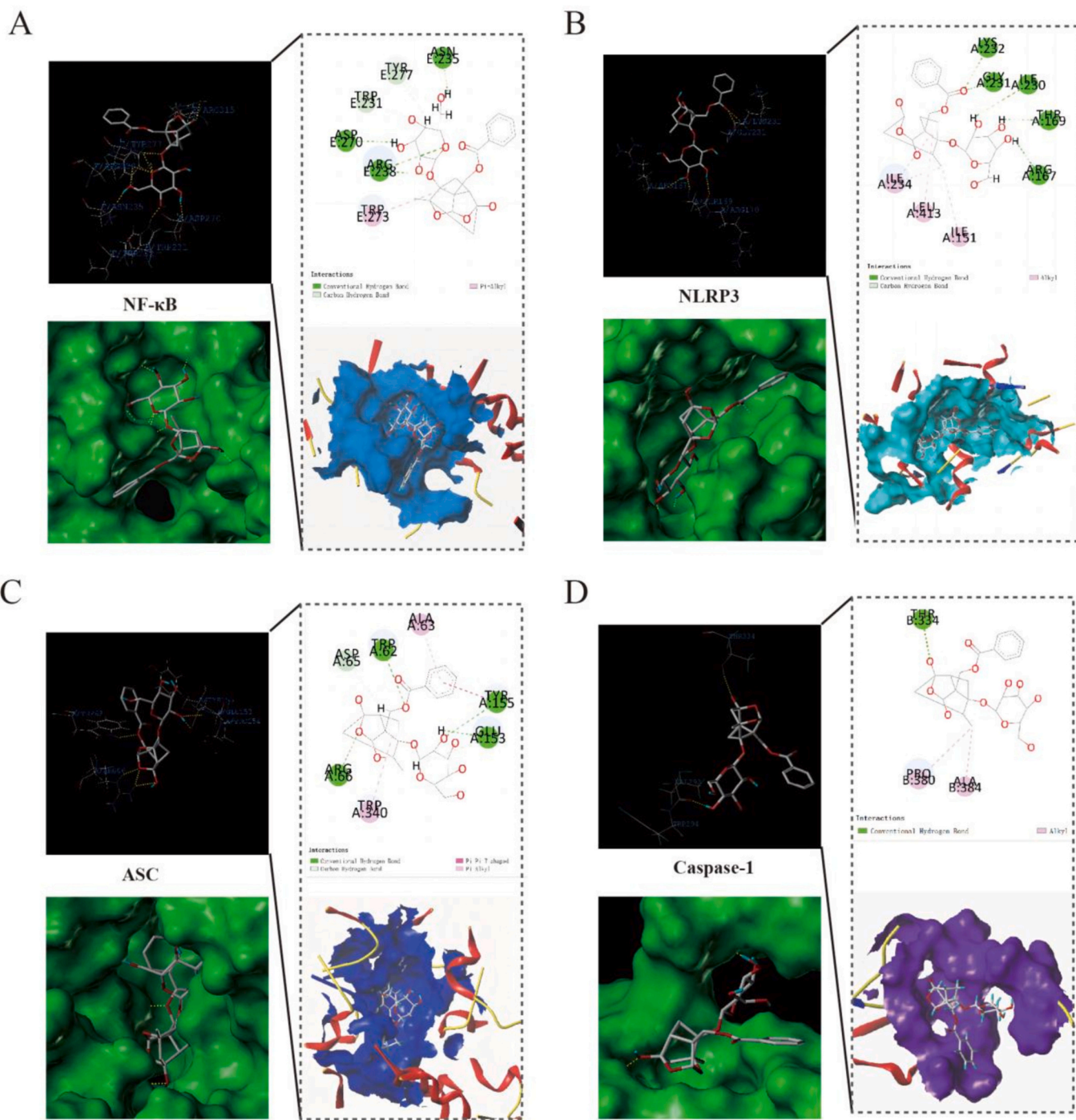
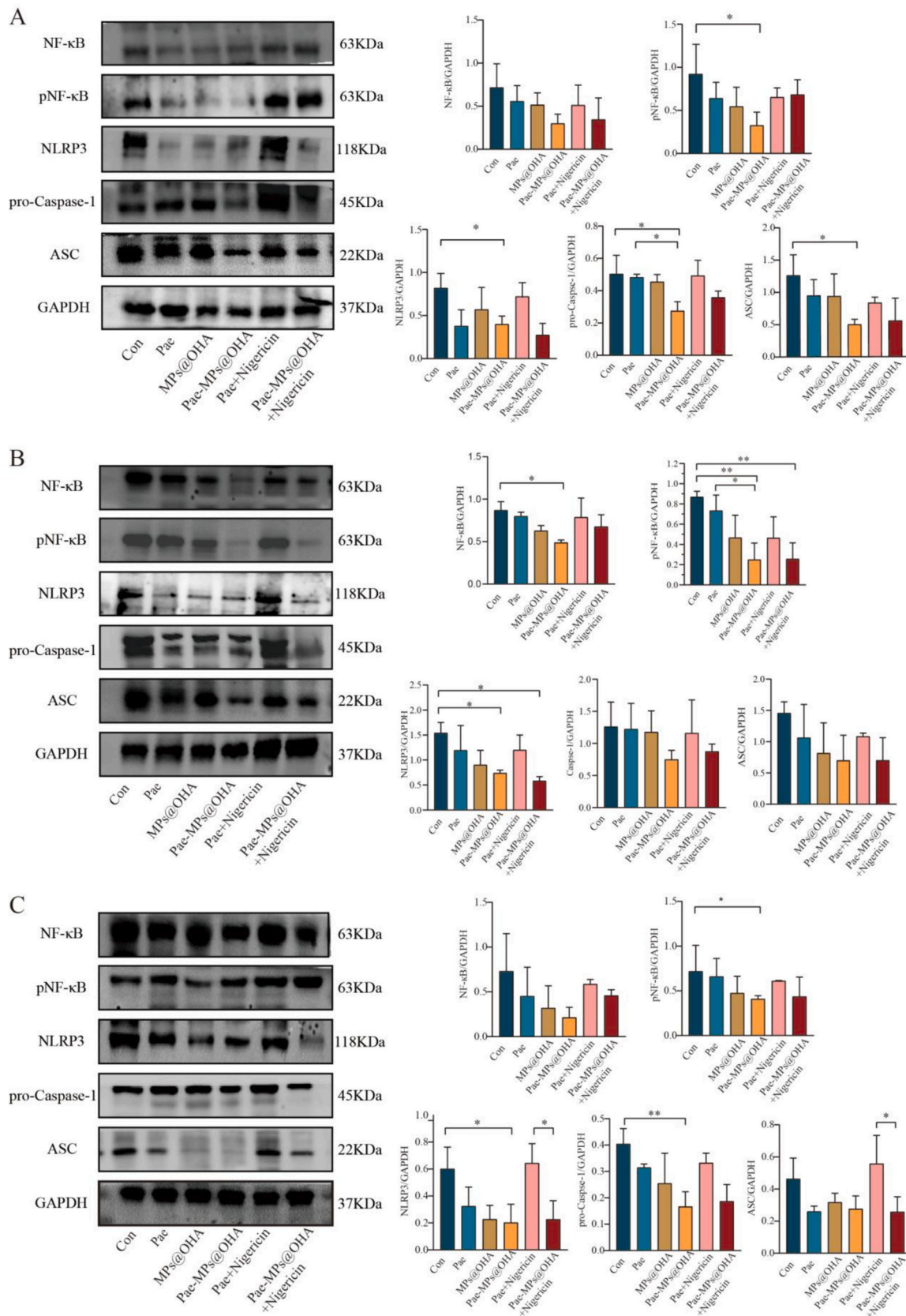


Fig. 9. Molecular docking studies of the Pae binding to NF-κB/NLRP3/Caspase-1/ASC proteins.

three-dimensional network structure and large network aperture, which has good water absorption and drug loading properties. This method was also used to prepare hydrogels in Hao Yang’s research [24]. Moreover, the drug delivery carrier of the Pae was broadened, which can make the Pae directly target wound cells to play a role. Particle size, PDI, and zeta potential are key indicators for evaluating microspheres [25,26]. Generally speaking, the particle size of hydrogel microspheres used for drug carriers or medical applications is relatively stable between several microns and hundreds of microns [25,26]. The particle size of the Pae-MPs was  $6.84 \pm 0.51 \mu\text{m}$ , which belongs to the best range, and its particle size was uniform and good stability. Danaei et al. reported that the PDI value is higher than 0.1 and lower than 0.3,

polydispersity is acceptable [27], the results of our study were consistent with those of Danaei et al. Zeta potential is one of the factors reflecting the stability of particles. When its absolute value is greater than or equal to 25 mV, it indicates good stability [28]. In our study, the absolute values of the Pae-MPs potentials were both  $>25$ , indicating good stability. Microsphere drug delivery technology is beneficial to the continuous release of active ingredients, reduce repeated administration and improve the bioavailability of drugs.

For wound dressings, regular gel pores and network structure are conducive to the absorption of exudates and the migration of cells, thus promoting wound healing [29,30]. In this study, both OHA and the Pae-MPs@OHA hydrogels demonstrated typical porous network



**Fig. 10.** The Pae-MPs@OHA hydrogels regulates the NF-κB/NLRP3 pathway. (A–C) The protein expression changes and statistical analysis of NF-κB, pNF-κB, NLRP3 and pro-caspase-1 at different time points (on days 10, 14, and 17) after trauma in each group. \* $p < 0.05$ , \*\* $p < 0.01$ .

morphology, with relatively uniform pores and orderly arrangement. SEM results also showed that the Pae-MPs could be loaded into the three-dimensional pores of OHA crosslinked hydrogels. The FTIR results further showed that the Pae was successfully modified on the PDA-MPs microspheres. Among the hydrogel dressings to promote wound healing, the drug should have good sustained release performance [31,32]. We observed that the Pae-MPs@OHA can achieve continuous release of the Pae for 96 h, and reach 64.8 % release rate at 24 h. It can not only play the therapeutic effect of the Pae, but also reduce the number of dressing changes and avoid the pain during dressing changes. The successful encapsulation of the Pae by the PDA-MPs was further verified. It lays a theoretical foundation for the application of the Pae-MPs@OHA.

Good adhesion properties are also necessary to facilitate the wound repair process [33,34]. The hydrogel adheres to the surface of the skin, maintaining a solid structure under external pressure to protect damaged wound tissues. In the preparation flow chart of the Pae-MPs@OHA, we observed that it can be adhered to the bottom of the centrifugal tube, which had good adhesion. The storage modulus ( $G'$ ) of the MPs@OHA hydrogels and the Pae-MPs@OHA hydrogels were higher than the loss modulus ( $G''$ ) in the range of 0.1–4.64 Hz and 0.1–3.16 Hz, respectively. The rheological tests showed that the Pae-MPs@OHA hydrogels had relatively stable overall properties and could maintain gel status. The Pae-MPs@OHA hydrogels can form a barrier on the surface of the damaged wound tissue to protect it from secondary injury.

The safety of dressing is a prerequisite for wound application [35]. The live/dead cell staining results of the Pae-MPs@OHA co-cultured with L929 cells suggested that the Pae-MPs@OHA had no cytotoxicity. The results of CCK-8 cells expressed that the Pae-MPs@OHA coculture with L929 cells could promote cell proliferation. It has been reported when the biomaterial is co-cultured with cells, the cell survival rate is >70 %, which indicates that the material has good biocompatibility [36]. This study confirmed that the Pae-MPs@OHA hydrogels had the ability to promote cell migration in vitro through cell scratch experiments. In vivo degradation experiments also proved that the Pae-MPs@OHA hydrogels had a stable degradation rate and can be used as a drug or cell carrier in vivo. This study displayed that the Pae-MPs@OHA had good biocompatibility. The reason may be that DA and HA are from nature and have no toxic effect on the human body. Meanwhile, it is also attributed to the fact that the anti-inflammatory drug molecules used in this study belong to the dual use of food and medicine.

An important reason for the difficulty of wound healing is that the wound remains in a state of high inflammation. M1 giant cells secrete a large number of pro-inflammatory factors such as TNF- $\alpha$  and IFN- $\gamma$ . These factors accumulate at the wound site, which in turn further promote the polarization of giant cells into M1 phenotype, which cannot be resolved during the inflammatory phase. Therefore, we carried out the binding experiment of TNF- $\alpha$  and IFN- $\gamma$  in vitro. It was proved that the Pae-MPs@OHA hydrogels had strong isolation effect on TNF- $\alpha$  and IFN- $\gamma$ . Due to the good biocompatibility and anti-inflammatory ability of the Pae-MPs@OHA, which was applied to the acute full-layer defect wound model in rats to further verify the effect of the Pae-MPs@OHA on wound healing. The wound healing rate of the Pae-MPs@OHA group was significantly different from that of the control group on days 4 and 8 ( $p < 0.05$ ). After 12 days, there was no significant difference in wound healing rate among all groups. It is speculated that the hydrogels as a carrier has good biocompatibility, can cover the wound to form a wet environment, effectively absorb the wound exudate, and play a role in protecting the wound. Studies have also reported that oxidized hyaluronic acid in hydrogels can promote cell migration and proliferation to a certain extent, thus accelerating wound healing [37,38].

An important reason for the delay in wound healing is the persistence of inflammation in the wound, which leads to the stagnation of healing [39,40]. The results of mice experiments indicated that the Pae-MPs@OHA could reduce the inflammatory reaction of wound surface, and the MPs@OHA and the Pae play a synergistic role in promoting

wound healing. In the case of excessive wound inflammation, the curative effect of the Pae-MPs@OHA was more significant. It was noted that there was no significant difference in the expression of IL-1 $\beta$  between each group on the 14th day. This phenomenon was reversed with the prolongation of time, confirming that the anti-inflammatory effect of the Pae-MPs@OHA hydrogels were dominated by the Pae. It was also confirmed that the levels of TNF- $\alpha$  and IL-1 $\beta$  in the wound tissues were evidently decreased in the later stage of wound healing. Excessive wound inflammation not only affects the inflammatory stage, but also interferes with the progress of subsequent proliferative and remodeling stages. During the wound remodeling phase, cells in the wound reshape the extracellular matrix by secreting collagen [41], and the maturation and deposition of collagen can accelerate the wound process. This study confirmed that the Pae-MPs@OHA can accelerate collagen maturation and promote the progress of wound remodeling. After injection of nigericin, the inflammatory stage of the wound was excessively prolonged, which seriously affected the progress of the subsequent proliferation and remodeling stage, and it was difficult to form collagen. Therefore, in the whole process of wound healing, effective control of inflammatory stage is very important for the subsequent healing process.

During the inflammatory phase of the wound, multiple immune cells are activated and participate in the entire inflammatory process [42,43]. Macrophages, as the main immune cells in wound healing, play an important role in the healing process [44]. The imbalance of macrophage function and phenotype in the wound tissues is the main reason for prolonging the inflammatory period of wound [45,46]. Therefore, we measured the number and function of macrophages in the wound tissues of each group. In this study, we found that the Pae-MPs@OHA can promote the transformation of M1 phenotype to M2 phenotype in the wound tissues, and inhibit the function of M1 macrophages. In addition, the Pae-MPs@OHA and the Pae-MPs@OHA + nigericin groups had better regulation of macrophage phenotype on the 10th and 14th, which may be related to the OHA and the Pae components of the Pae-MPs@OHA hydrogels. Yan et al. also reported that the dynamics and plasticity of macrophages enable them to change in response to local microenvironmental stimuli or signals [47]. However, in acute wounds, the polarization function of macrophages is impaired, which leads to the aggregation and activation of M1 macrophages, the inflammatory state of wounds increases and the healing process is delayed [48,49]. Therefore, it is very important to stop inflammation in time by targeted regulation of M1/M2 polarization of macrophages, so as to improve the speed of wound repair.

We further explored the regulatory mechanism of the Pae-MPs@OHA on wound macrophages. As the most common nuclear transcription factor, NF- $\kappa$ B is composed of I $\kappa$ B $\alpha$ , p65 and p50 [50]. Normally, NF- $\kappa$ B is inactivated in the cytoplasm. After stimulation, it causes degradation of I $\kappa$ B, and p65 is released into the nucleus to regulate the expression of target genes by binding to the upstream promoter region of target genes at the transcriptional level, and is involved in the occurrence and development of various diseases [51]. Studies have shown that NF- $\kappa$ B can activate inflammasome in macrophages [52]. The activated inflammasome NLRP3 binds to ASC and caspase-1, and plays a pro-inflammatory role by transforming pre-IL-1 $\beta$  and pre-IL-18 into IL-1 $\beta$  and IL-18 [52]. In inflammatory diseases, multi-pathway inhibition of NF- $\kappa$ B can effectively reduce the inflammatory signal transduction mediated by NLRP3 [53–55]. Zhang et al. also proved that inhibiting NF- $\kappa$ B in bone marrow-derived macrophages can reduce the polarization of M1 macrophages and increase the proportion of M2 cells [56]. Based on this, molecular docking was used to reveal the binding activity between the Pae and NF- $\kappa$ B, NLRP3, ASC and caspase-1 proteins. The results displayed that the Pae could bind through a variety of covalent bonds and had good activity. Studies have shown that reducing the expression of pro-caspase-1 can inhibit the activation of caspase-1, thereby reducing the degree of inflammatory response [57]. Western blot results further confirmed that the Pae-MPs@OHA could

reduce the expression of NF- $\kappa$ B, pNF- $\kappa$ B, NLRP3, ASC and pro-caspase-1. This phenomenon indicated that the Pae played a synergistic role with the MPs@OHA. It was also related to the sustained release of the Pae from the Pae-MPs@OHA.

## 5. Conclusion

In short, the Pae, the PDA-MPs and OHA were used as raw materials to prepare the Pae-MPs@OHA dressing with good biocompatibility, mechanical stability, uniform particle size and potential to promote wound healing. Meanwhile, it was found that the microspheres were conducive to drug delivery and release. In vivo experiments confirmed that the Pae-MPs@OHA can inhibit NF- $\kappa$ B/NLRP3 signaling pathway, regulate the polarization of M1/M2 macrophages, accelerate the re-epithelization process of wound surface, reduce the infiltration of inflammatory cells and promote collagen deposition, further reduce the inflammatory reaction of wound and promote the healing of acute wound in rats. Therefore, a new type of the Pae-MPs@OHA hydrogels dressing was prepared for the first time in this study, which provided a new idea and experimental basis for the emergency treatment of acute defect wounds.

## Funding

This project was supported by the Shenyang Science and Technology Plan Project (22-315-6-17), National College Students Innovation and Entrepreneurship Training Program (20239005) and the Shenyang Natural Science Foundation Special Project (23-503-6-14).

## CRedit authorship contribution statement

**Jiarui Liu:** Writing – original draft, Visualization, Methodology. **Siqi Chen:** Methodology, Formal analysis, Data curation. **Zijing Zhang:** Methodology, Formal analysis, Data curation. **Xitong Song:** Methodology, Formal analysis, Data curation. **Zhiquan Hou:** Software, Methodology. **Ziyi Wang:** Software, Methodology. **Tao Liu:** Software, Methodology, Data curation. **Liqun Yang:** Writing – review & editing. **Yunen Liu:** Supervision, Resources, Formal analysis. **Zhonghua Luo:** Writing – review & editing, Project administration, Funding acquisition.

## Declaration of competing interest

The authors declare no conflicts of interest.

## Appendix A. Supplementary data

Supplementary data to this article can be found online at <https://doi.org/10.1016/j.ijbiomac.2024.137107>.

## Data availability

The authors do not have permission to share data.

## References

- J. Li, J. Long, Z. Zhao, Q. Wang, W. Bo, L. Ren, Y. Fan, P. Wang, Y. Cheng, B. Liu, X. Cheng, H. Xi, Procedural promotion of multiple stages in the wound healing process by graphene-spiky silica heterostructured nanoparticles, *Int. J. Nanomed.* 18 (2023) 6585–6599.
- A.J. Singer, Healing mechanisms in cutaneous wounds: tipping the balance, *Tissue Eng. Part B Rev.* 28 (2022) 1151–1167.
- C. Li, M.M. Xu, K. Wang, A.J. Adler, A.T. Vella, B. Zhou, Macrophage polarization and meta-inflammation, *Transl. Res.* 191 (2018) 29–44.
- J. Pajarinen, T. Lin, E. Gibon, Y. Kohno, M. Maruyama, K. Nathan, L. Lu, Z. Yao, S. B. Goodman, Mesenchymal stem cell-macrophage crosstalk and bone healing, *Biomaterials* 196 (2019) 80–89.
- M.K. Neog, F. Sultana, M. Rasool, Targeting RAW 264.7 macrophages (M1 type) with Withaferin—a decorated mannosylated liposomes induces repolarization via downregulation of NF- $\kappa$ B and controlled elevation of STAT-3, *Int. Immunopharmacol.* 61 (2018) 64–73.
- F. Ginhoux, J.L. Schultze, P.J. Murray, J. Ochando, S.K. Biswas, New insights into the multidimensional concept of macrophage ontogeny, activation and function, *Nat. Immunol.* 17 (2016) 34–40.
- X. Shan, P. Hu, L. Ni, L. Shen, Y. Zhang, Z. Ji, Y. Cui, M. Guo, H. Wang, L. Ran, K. Yang, T. Wang, L. Wang, B. Chen, Z. Yao, Y. Wu, Q. Yu, Serine metabolism orchestrates macrophage polarization by regulating the IGF1-p38 axis, *Cell. Mol. Immunol.* 19 (2022) 1263–1278.
- E. Kolaczowska, P. Kubes, Neutrophil recruitment and function in health and inflammation, *Nat. Rev. Immunol.* 13 (2013) 159–175.
- G. Erzioglu, T.L. Young-Pearse, Microglial function, INPP5D/SHIP1 signaling, and NLRP3 inflammasome activation: implications for Alzheimer's disease, *Mol. Neurodegener.* 18 (2023) 89.
- Q. Zhang, L. Shi, H. He, X. Liu, Y. Huang, D. Xu, M. Yao, N. Zhang, Y. Guo, Y. Lu, H. Li, J. Zhou, J. Tan, M. Xing, G. Luo, Down-regulating scar formation by microneedles directly via a mechanical communication pathway, *ACS Nano* 16 (2022) 10163–10178.
- Z. Yan, L. Xie, M. Li, M. Yuan, Y. Tian, D. Sun, Y. Zhang, L. Niu, Phytochemical components and bioactivities of novel medicinal food — peony roots, *Food Res. Int.* 140 (2021) 109902.
- L. Zhang, W. Wei, Anti-inflammatory and immunoregulatory effects of paeoniflorin and total glucosides of paeony, *Pharmacol. Ther.* 207 (2020) 107452.
- Y. Liang, J. He, B. Guo, Functional hydrogels as wound dressing to enhance wound healing, *ACS Nano* 15 (2021) 12687–12722.
- H. Cheng, Z. Shi, K. Yue, X. Huang, Y. Xu, C. Gao, Z. Yao, Y.S. Zhang, J. Wang, Sprayable hydrogel dressing accelerates wound healing with combined reactive oxygen species-scavenging and antibacterial abilities, *Acta Biomater.* 124 (2021) 219–232.
- M. Abazari, T. Akbari, M. Hasani, E. Sharifikolouei, M. Raoufi, A. Foroumadi, M. Sharifzadeh, L. Firoozpour, M. Khoobi, Polysaccharide-based hydrogels containing herbal extracts for wound healing applications, *Carbohydr. Polym.* 294 (2022) 119808.
- M.F.P. Graça, S.P. Miguel, C.S.D. Cabral, I.J. Correia, Hyaluronic acid-based wound dressings: a review, *Carbohydr. Polym.* 241 (2020) 116364.
- L. Feng, W. Shi, Q. Chen, H. Cheng, J. Bao, C. Jiang, W. Zhao, C. Zhao, Smart asymmetric hydrogel with integrated multi-functions of NIR-triggered tunable adhesion, self-deformation, and bacterial eradication, *Adv. Healthc. Mater.* 19 (2021) e2100784.
- A. Seth, H. Gholami Derami, P. Gupta, Z. Wang, P. Rath, R. Gupta, T. Cao, J. J. Morrissey, S. Singamaneni, Polydopamine-mesoporous silica core-shell nanoparticles for combined photothermal immunotherapy, *ACS Appl. Mater. Interfaces* 12 (2020) 42499–42510.
- S. Liu, J. Pan, J. Liu, Y. Ma, F. Qiu, L. Mei, X. Zeng, G. Pan, Dynamically PEGylated and borate-coordination-polymer-coated polydopamine nanoparticles for synergetic tumor-targeted, chemo-photothermal combination therapy, *Small* (2018) e1703968.
- X.Z. Yang, W. Wei, CP-25, a compound derived from paeoniflorin: research advance on its pharmacological actions and mechanisms in the treatment of inflammation and immune diseases, *Acta Pharmacol. Sin.* 41 (2020) 1387–1394.
- S.A. Eming, P. Martin, M. Tomic-Canic, Wound repair and regeneration: mechanisms, signaling, and translation, *Sci. Transl. Med.* 6 (2014) 265sr6.
- M. Sharifaghdam, E. Shaabani, R. Faridi-Majidi, S.C. De Smedt, K. Braeckmans, J. C. Fraire, Macrophages as a therapeutic target to promote diabetic wound healing, *Mol. Ther.* 30 (2022) 2891–2908.
- C. Qi, Q. Sun, D. Xiao, M. Zhang, S. Gao, B. Guo, Y. Lin, Tetrahedral framework nucleic acids/hyaluronic acid-methacrylic anhydride hybrid hydrogel with antimicrobial and anti-inflammatory properties for infected wound healing, *Int. J. Oral Sci.* 16 (2024) 30.
- H. Yang, L. Song, B. Sun, D. Chu, L. Yang, M. Li, H. Li, Y. Dai, Z. Yu, J. Guo, Modulation of macrophages by a paeoniflorin-loaded hyaluronic acid-based hydrogel promotes diabetic wound healing, *Mater. Today Bio* 12 (2021) 100139.
- A. Arif, N. Ameer, M. Hanif, K. Mahmood, M. Arif, A.A. Shah, H.R. Nisar, B. Khan, W.S. Khan, Lipase-copper complex/chitosan microspheres; loaded with attapulgite used for the treatment of *E. coli*-induced diarrhea, *Int. J. Biol. Macromol.* 277 (2024) 134167.
- Y. Pang, P. Lin, Z. Chen, M. Zhou, D. Yang, H. Lou, X. Qiu, Preparation, characterization, and adsorption performance of porous polyamine lignin microsphere, *Int. J. Biol. Macromol.* 253 (2023) 127026.
- M. Danaei, M. Dehghankhold, S. Ataei, F. Hasanzadeh Davarani, R. Javanmard, A. Dokhani, S. Khorasani, M.R. Mozafari, Impact of particle size and polydispersity index on the clinical applications of lipidic nanocarrier systems, *Pharmaceutics* 10 (2018) 57.
- A. Pareek, R. Kothari, A. Pareek, Y. Ratan, P. Kashania, V. Jain, P. Jeandet, P. Kumar, A.A. Khan, A.M. Alanazi, M.M. Gupta, Development of a new inhaled swellable microsphere system for the dual delivery of naringenin-loaded solid lipid nanoparticles and doxofylline for the treatment of asthma, *Eur. J. Pharm. Sci.* 193 (2024) 106642.
- Z. Dong, D. Wu, H. Engqvist, J. Luo, C. Persson, Silk fibroin hydrogels induced and reinforced by acidic calcium phosphate — a simple way of producing bioactive and drug-loadable composites for biomedical applications, *Int. J. Biol. Macromol.* 193 (2021) 433–440.
- M. Hamidi, A. Azadi, P. Rafiei, Hydrogel nanoparticles in drug delivery, *Adv. Drug Deliv. Rev.* 60 (2008) 1638–1649.

- [31] S. Hezari, A. Olad, A. Dilmaghani, Modified gelatin/iron-based metal-organic framework nanocomposite hydrogel as wound dressing: synthesis, antibacterial activity, and *Camellia sinensis* release, *Int. J. Biol. Macromol.* 218 (2022) 488–505.
- [32] Y. Chen, X. Wang, S. Tao, Q. Wang, P.Q. Ma, Z.B. Li, Y.L. Wu, D.W. Li, Research advances in smart responsive-hydrogel dressings with potential clinical diabetic wound healing properties, *Mil. Med. Res.* 10 (2023) 37.
- [33] N. Rauner, M. Meuris, M. Zoric, J.C. Tiller, Enzymatic mineralization generates ultrastiff and tough hydrogels with tunable mechanics, *Nature* 543 (2017) 407–410.
- [34] G.G.G. Perera, D.F. Argenta, T. Caon, The rheology of injectable hyaluronic acid hydrogels used as facial fillers: a review, *Int. J. Biol. Macromol.* 268 (2024) 131880.
- [35] M. Wu, H. Liu, Y. Zhu, F. Chen, Z. Chen, L. Guo, P. Wu, G. Li, C. Zhang, R. Wei, L. Cai, Mild photothermal-stimulation based on injectable and photocurable hydrogels orchestrates immunomodulation and osteogenesis for high-performance bone regeneration, *Small* 19 (2023) e2300111.
- [36] N.T. Nguyen, L.V. Nguyen, N.M. Tran, D.T. Nguyen, T.N. Nguyen, H.A. Tran, N. N. Dang, T.V. Vo, T.H. Nguyen, The effect of oxidation degree and volume ratio of components on properties and applications of in situ cross-linking hydrogels based on chitosan and hyaluronic acid, *Mater. Sci. Eng. C Mater. Biol. Appl.* 103 (2019) 109670.
- [37] W. Tan, T. Long, Y. Wan, B. Li, Z. Xu, L. Zhao, C. Mu, L. Ge, D. Li, Dual-drug loaded polysaccharide-based self-healing hydrogels with multifunctionality for promoting diabetic wound healing, *Carbohydr. Polym.* 312 (2023) 120824.
- [38] Y. Wang, Y. Zhang, Y.P. Yang, M.Y. Jin, S. Huang, Z.M. Zhuang, T. Zhang, L.L. Cao, X.Y. Lin, J. Chen, Y.Z. Du, J. Chen, W.Q. Tan, Versatile dopamine-functionalized hyaluronic acid-recombinant human collagen hydrogel promoting diabetic wound healing via inflammation control and vascularization tissue regeneration, *Bioact. Mater.* 35 (2024) 330–345.
- [39] X.D. Zhao, D.N. Pei, Y.X. Yang, Green tea derivative driven smart hydrogels with desired functions for chronic diabetic wound treatment, *Adv. Funct. Mater.* 31 (2021) 18.
- [40] Z.L. Tu, M. Chen, M. Wang, Engineering bioactive M2 macrophage-polarized anti-inflammatory, antioxidant, and antibacterial scaffolds for rapid angiogenesis and diabetic wound repair, *Adv. Funct. Mater.* 31 (2021) 30.
- [41] J. Wu, Z. Xiao, A. Chen, H. He, C. He, X. Shuai, X. Li, S. Chen, Y. Zhang, B. Ren, J. Zheng, J. Xiao, Sulfated zwitterionic poly(sulfobetaine methacrylate) hydrogels promote complete skin regeneration, *Acta Biomater.* 71 (2018) 293–305.
- [42] X. Zhou, S. Wahane, M.S. Friedl, M. Kluge, C.C. Friedel, K. Avrampou, V. Zachariou, L. Guo, B. Zhang, X. He, R.H. Friedel, H. Zou, Microglia and macrophages promote corraling, wound compaction and recovery after spinal cord injury via Plexin-B2, *Nat. Neurosci.* 23 (2020) 337–350.
- [43] Y. Yang, C. Chu, L. Liu, C. Wang, C. Hu, S. Rung, Y. Man, Y. Qu, Tracing immune cells around biomaterials with spatial anchors during large-scale wound regeneration, *Nat. Commun.* 14 (2023) 5995.
- [44] X. Huang, L. Zheng, Y. Zhou, S. Hu, W. Ning, S. Li, Z. Lin, S. Huang, Controllable adaptive molybdate-oligosaccharide nanoparticles regulate M2 macrophage mitochondrial function and promote angiogenesis via PI3K/HIF-1 $\alpha$ /VEGF pathway to accelerate diabetic wound healing, *Adv. Healthc. Mater.* 13 (2024) e2302256.
- [45] R.D. Stout, J. Suttles, Immunosenescence and macrophage functional plasticity: dysregulation of macrophage function by age-associated microenvironmental changes, *Immunol. Rev.* 205 (2005) 60–71.
- [46] S. He, Z. Li, L. Wang, N. Yao, H. Wen, H. Yuan, J. Zhang, Z. Li, C. Shen, A nanoenzyme-modified hydrogel targets macrophage reprogramming-angiogenesis crosstalk to boost diabetic wound repair, *Bioact. Mater.* 35 (2024) 17–30.
- [47] J. Yan, G. Tie, S. Wang, A. Tutto, N. DeMarco, L. Khair, T.G. Fazzio, L.M. Messina, Diabetes impairs wound healing by Dnmt1-dependent dysregulation of hematopoietic stem cells differentiation towards macrophages, *Nat. Commun.* 9 (2018) 33.
- [48] H. Park, T.V. Patil, S.D. Dutta, J. Lee, K. Ganguly, A. Randhawa, H. Kim, K.T. Lim, Extracellular matrix-bioinspired anisotropic topographical cues of electrospun nanofibers: a strategy of wound healing through macrophage polarization, *Adv. Healthc. Mater.* 13 (2024) e2304114.
- [49] X. Huang, L. Zheng, Y. Zhou, S. Hu, W. Ning, S. Li, Z. Lin, S. Huang, Controllable adaptive molybdate-oligosaccharide nanoparticles regulate M2 macrophage mitochondrial function and promote angiogenesis via PI3K/HIF-1 $\alpha$ /VEGF pathway to accelerate diabetic wound healing, *Adv. Healthc. Mater.* 13 (2024) e2302256.
- [50] S.Z. Li, Q.P. Shu, H.M. Zhou, Y.Y. Liu, M.Q. Fan, X.Y. Liang, L.Z. Qi, Y.N. He, X. Y. Liu, X.H. Du, X.C. Huang, Y.Z. Chen, R.L. Du, Y.X. Liang, X.D. Zhang, CLK2 mediates I $\kappa$ B $\alpha$ -independent early termination of NF- $\kappa$ B activation by inducing cytoplasmic redistribution and degradation, *Nat. Commun.* 15 (2024) 3901.
- [51] T.J. Florio, R.K. Lokareddy, D.P. Yeggoni, R.S. Sankhala, C.A. Ott, R.E. Gillilan, G. Cingolani, Differential recognition of canonical NF- $\kappa$ B dimers by importin  $\alpha$ 3, *Nat. Commun.* 13 (2022) 1207.
- [52] S. Wang, M. Lu, W. Wang, S. Yu, R. Yu, C. Cai, Y. Li, Z. Shi, J. Zou, M. He, W. Xie, D. Yu, H. Jin, H. Li, W. Xiao, C. Fan, F. Wu, Y. Li, S. Liu, Macrophage polarization modulated by NF- $\kappa$ B in polylactide membranes-treated peritendinous adhesion, *Small* 18 (2022) e2104112.
- [53] W. Sun, Q. Wang, R. Zhang, N. Zhang, Ketogenic diet attenuates neuroinflammation and induces conversion of M1 microglia to M2 in an EAE model of multiple sclerosis by regulating the NF- $\kappa$ B/NLRP3 pathway and inhibiting HDAC3 and P2X7R activation, *Food Funct.* 14 (2023) 7247–7269.
- [54] Z. Li, H. Pan, J. Yang, D. Chen, Y. Wang, H. Zhang, Y. Cheng, Xuanfei Baidu formula alleviates impaired mitochondrial dynamics and activated NLRP3 inflammasome by repressing NF- $\kappa$ B and MAPK pathways in LPS-induced ALI and inflammation models, *Phytomedicine* 108 (2023) 154545.
- [55] X. Zhang, W. Ning, G. Gao, Y. Zhou, X.B. Duan, X. Li, D. Li, R. Guo, Bazedoxifene attenuates intestinal injury in sepsis by suppressing the NF- $\kappa$ B/NLRP3 signaling pathways, *Eur. J. Pharmacol.* 947 (2023) 175681.
- [56] P. Zhang, P. Wu, U.Z. Khan, Z. Zhou, X. Sui, C. Li, K. Dong, Y. Liu, L. Qing, J. Tang, Exosomes derived from LPS-preconditioned bone marrow-derived MSC modulate macrophage plasticity to promote allograft survival via the NF- $\kappa$ B/NLRP3 signaling pathway, *J. Nanobiotechnol.* 21 (2023) 332.
- [57] F. Wang, Q. Liang, Y. Ma, M. Sun, T. Li, L. Lin, Z. Sun, J. Duan, Silica nanoparticles induce pyroptosis and cardiac hypertrophy via ROS/NLRP3/Caspase-1 pathway, *Free Radic. Biol. Med.* 182 (2022) 171–181.